3-D Joint Inversion of Magnetotelluric and Airborne Tipper Data: A case study from the Morrison porphyry Cu-Au-Mo deposit, British Columbia, Canada

Benjamin Lee[1], Martyn Unsworth[1], Juliane Hübert[1,2], Jeremy Richards[1], Jean M. Legault[3]

[1]*University of Alberta, Edmonton, CA*

[2]*Current address: University of Edinburgh, Edinburgh, U.K.*

[3]*Geotech Ltd., Aurora, CA*

Corresponding author: Benjamin Lee (email: blee3@ualberta.ca)

Abstract

Z-axis tipper electromagnetic (ZTEM) and broadband magnetotelluric (MT) data were used to determine three-dimensional (3-D) electrical resistivity models of the Morrison porphyry Cu-Au-Mo deposit in British Columbia. ZTEM data are collected with a helicopter, thus allowing rapid surveys with uniform spatial sampling. Ground-based MT surveys can achieve a greater exploration depth than ZTEM, but data collection is slower and can be limited by difficult terrain. The airborne ZTEM tipper data and the ground MT tipper data show good agreement at the Morrison deposit despite differences in the data collection method, spatial sampling and collection date. Resistivity models derived from individual inversions of the ZTEM tipper data and MT impedance data contain some similar features, but the ZTEM model appears to lack resolution below a depth of 1 km and the MT model suffers from non-uniform and relatively sparse spatial sampling. The joint ZTEM-MT inversion solves these issues by combining the dense spatial sampling of the airborne ZTEM technique and the deeper penetration of the lower frequency MT data. The resulting joint resistivity model correlates well with the known geology and distribution of alteration at the Morrison deposit. Higher resistivity is associated with the potassic alteration zone and volcanic country rocks, whereas areas of lower resistivity agree with known faults and sedimentary units. The pyrite halo and ≥0.3 % Cu zone have the moderate resistivity that is expected of disseminated sulfides. The joint ZTEM-MT inversion provides an improved resistivity model by enhancing the lateral and depth resolution of resistivity features compared to the individual ZTEM and MT inversions. This case study shows that a joint ZTEM-MT approach effectively images the interpreted mineralized zone at the Morrison deposit and could be beneficial in exploration for disseminated sulfides at other porphyry deposits.

Keywords

Joint inversion, Airborne electromagnetic

1. Introduction

Electromagnetic (EM) geophysical surveys are widely used to detect metallic sulfide deposits based on their electrical resistivity contrasts with the host rock. Massive sulfides typically have low resistivity values of 0.1 – 1 Ωm (Palacky, 1988) that are readily detected with the time domain electromagnetic method (TDEM). Deposits containing disseminated sulfides, where the sulfide minerals occur as individual grains within the rock matrix, have a higher resistivity and smaller resistivity contrasts with the host rock that may not be easily detected with TDEM since limited electric current is induced in the more resistive target (Kaminski et al., 2010; Paré and Legault, 2010). Thus detection of disseminated sulfides based on resistivity contrasts benefits from the use of frequency domain EM methods that can detect targets with a higher resistivity, which often means a lower resistivity contrast with the host rock. Methods that can be used include the ground-based magnetotelluric (MT) technique which measures naturally-occurring electric and magnetic fields to determine subsurface resistivity at greater depths than controlled source techniques. However, the electric field sensors in an MT survey require ground contact, so MT surveys are more time consuming and cannot easily achieve the same spatial coverage as airborne EM (AEM) methods. The airborne Z-Axis Tipper Electromagnetic (ZTEM) method is described by Lo and Zang (2008), and is a development of the Audio-Frequency (AFMAG) technique originally proposed by Ward (1959). The ZTEM technique only uses magnetic field measurements and can thus be made from an airborne platform. However, the lack of electric field data means that ZTEM is not as sensitive as MT impedance data to absolute resistivity values. In addition, tipper data is non-zero only in the presence of lateral changes in resistivity (i.e. 2-D or 3-D resistivity structures). Combining the greater depth of penetration of

MT with the high spatial sampling of airborne ZTEM data has the possibility to produce an improved exploration strategy (Holtham, 2012).

This paper describes a case study of how MT impedance and ZTEM tipper data can be jointly used in mineral exploration. As the ZTEM and MT techniques share similarities in processing and inversion, there have been several previous studies of simultaneously inverting these data to obtain an improved resistivity model (Holtham, 2012; Sasaki et al., 2014; Wannamaker and Legault, 2014; Sattel and Witherly, 2015). ZTEM case studies have been published for several types of mineral deposits including porphyry Cu, massive sulfide, and unconformity uranium, and there is interest in incorporating additional geophysical information to further improve the ZTEM results (Kaminski et al., 2010; Paré et al., 2012; Orta et al., 2013, Hübert et al., 2015; Legault et al., 2016). This paper focuses on porphyry deposits because their geophysical signatures can vary greatly depending on the local geology and erosion history. Previous studies have shown that these deposits could have a distinct electrical resistivity signature from their host rock.

The Morrison porphyry Cu-Au-Mo deposit in British Columbia, Canada, was chosen for this study because a ZTEM dataset was available, the deposit was accessible for a ground-based MT survey, and the mineralization is known to extend to a depth of at least 400 m (Simpson, 2007) providing a realistic test of the penetration depth of MT and ZTEM data. After completion of the MT survey, the MT and ZTEM data were separately and jointly inverted to obtain electrical resistivity models. These models show that data from these methods can be used to map electrical resistivity contrasts associated with porphyry Cu deposits. The individual inversions of ZTEM tipper and MT impedance data resulted in resistivity models with similar features even though the datasets differ in acquisition, frequency range, and spatial sampling.

Past studies have shown that different types of geophysical data need to be appropriately weighted in a joint inversion (Mackie et al., 2007; Commer and Newman, 2009). This ensures that the resulting model is not biased by a disparity in data quantity or resolution. In this case study of the Morrison deposit the total number of ZTEM data points is two orders of magnitude greater than the number of MT data points. The ZTEM and MT data were assigned different weights to achieve a comparable data fit and to derive a resistivity model that was consistent with both datasets.

2. Electrical Resistivity of Porphyry Deposits

Porphyry Cu deposits are mostly formed by hydrothermal fluids exsolved from arc magmas emplaced in the upper crust above subduction zones (Sillitoe, 1972, 1973, 2010; Richards, 2003; Cooke et al., 2005). The magmas in this setting originate from partial melting of the metasomatized mantle wedge between the subducting oceanic plate and overriding plate. Voluminous emplacement of these hydrous, moderately oxidized arc magmas in mid- to upper crustal batholithic intrusions results in volatile saturation and partitioning of Cu and other metals (Mo ± Au) into a saline hydrothermal fluid phase. Metals are precipitated as sulfide minerals to form ore deposits where ascent of these fluids is focused into narrow cupola zones extending from a few kilometers depth above the source batholith to subvolcanic levels. Cooling and wallrock reactions cause precipitation of chalcopyrite and molybdenite in quartz-sulfide veins and as disseminations in potassic altered rock (with hydrothermal K-feldspar, biotite, magnetite, anhydrite). As these fluids ascend and cool further, they become increasingly acidic, resulting in progressive phyllic (quartz-sericite-pyrite), argillic, and advanced argillic (clay, alunite, diaspore, residual quartz) alteration (Sillitoe, 2010; Richards, 2011). Alteration and sulfide minerals are thus zoned vertically and laterally in a characteristic pattern typically centered on a shallow subvolcanic intrusive complex, although this pattern may be modified by later structural disturbance (Lowell and Guilbert, 1970). Post-formation uplift and erosion progressively denudes shallow level (epithermal) hydrothermal alteration and volcanic rocks, exposing the underlying subvolcanic rocks and porphyry mineralization, and then eventually the underlying barren batholith. Burial by younger volcanic and sedimentary rocks can preserve various levels of the system, and presents a major challenge for mineral exploration. Whereas in many parts of the world, including the Cordillera of British Columbia, exposed porphyry systems have mostly been discovered and tested, considerable potential remains for the discovery of unexposed or buried deposits. Geophysical methods (i.e. magnetics, induced polarization, EM methods) can be used for the detection of such systems by searching for contrasts between the physical properties of rocks associated with alteration and mineralization and those of surrounding country rocks. Methods that can resolve such contrasts at depth or below cover are thus particularly valuable in modern mineral exploration.

EM exploration techniques are well suited to this purpose because they are sensitive to electrical resistivity contrasts associated with alteration and mineralization in porphyry deposits (Holliday and Cooke, 2007; Mitchinson et al., 2013). A pattern of hydrothermal alteration in a generalized porphyry deposit is shown in Figure 1A and the associated mineralization in 1B. Because the alteration zones are formed under particular conditions of temperature and salinity, the spatial and depth extent of each zone varies for each deposit (Sillitoe, 2010; Richards, 2011).

Figure 1C shows the expected resistivity values at different parts of the generalized deposit. The potassic zone consists of crystalline intrusive rock, and can be detected if its resistivity differs from the host rock. Intrusive rocks typically have a high resistivity because limited pore space restricts the flow of electric current. For instance, a deposit hosted by young, porous sedimentary rock should have a resistive anomaly corresponding to the porphyritic stock. Fresh intrusive rocks typically have resistivities in the range 1000 - 5000 Ωm depending on the degree of fracturing, which decreases resistivity (Figure 1C). Disseminated sulfides in potassic-altered intrusive rocks and wallrocks may lower the resistivity relative to fresh rocks, but only moderately because sulfide abundance is not high (typically 1–2 vol.%) and is generally not in connected form (veins and veinlets predominantly consist of resistive quartz with only minor interspersed sulfides, albeit consisting of potentially economically valuable Cu-Fe- and Mo-sulfides). In contrast, the phyllic alteration zone is characterized by abundant disseminated and veinlet pyrite (up to 20 vol.%), with distinctly lower bulk resistivity depending on the amount and interconnectivity of the sulfide grains. Shallow level argillic and advanced argillic alteration typically has relatively low resistivity due to the presence of conductive clay minerals.

The resistivity profile across a porphyry system is thus dependent on the erosion level of the deposit (Figure 1C). An uneroded deposit can exhibit a low resistivity near-surface signature due to the presence of clay minerals in the argillic zone, but if the deposit has been eroded down to the porphyry level, then the more resistive potassic zone will dominate the resistivity profile over the deposit. ZTEM and MT surveys are particularly useful for studying uneroded deposits, or those located below cover, because they are capable of exploration to greater depths than controlled source EM methods.

The resistivity of the sulfide-rich phyllic and potassic zones can vary by orders of magnitude depending on the sulfide concentration and distribution. Nelson and Van Voorhis (1983) collected 109 in-situ resistivity measurements at four porphyry Cu deposits and showed that resistivity is inversely proportional to sulfide content (Figure 2). The mineralization was classified as disseminated or in discontinuous veins for about 3 wt.% sulfide and below. In this case, Nelson and Van Voorhis (1983) found that the resistivity was high (> 100 Ωm) and variable. At 3 – 20 wt.% the sulfides are increasingly vein-hosted, and the resistivity decreases to below 10 Ωm for samples approaching 20 wt.% sulfide. Although this study did not include massive sulfide samples, these would generally be above 50% weight sulfides, and have a very low resistivity (< 1 Ωm). This shows that there can be up to three orders of magnitude variability in resistivity depending on the concentration of sulfide mineralization. Porphyry deposits can contain a large volume of disseminated sulfides with bulk resistivity in the range 100 to 1000 Ωm. This is a relatively high resistivity compared to massive sulfides and sulfide mineralization in well-connected veins where bulk resistivities are 1 to 10 Ωm. More importantly, detection of disseminated sulfides could be a challenge for EM techniques if the sulfides are relatively resistive and buried under cover. This is motivation to study whether the natural source ZTEM and MT methods can detect disseminated sulfide zones that may not appear as obvious, highly conductive targets. It should be noted that the induced polarization (IP) method is sensitive to chargeability and is thus effective at detecting disseminated sulfides (Seigel et al., 2007). As this is a proven method and is related to a different physical property, it is not the focus of this study.

3. Magnetotelluric and Z-axis tipper electromagnetic Theory

AEM surveys are a practical choice for mineral exploration because they can cover large areas quickly and are relatively inexpensive. Controlled source AEM systems have been extensively used in mineral exploration and are effective for imaging near-surface targets. Legault (2015) provides a comprehensive review of controlled source AEM methods in the time and frequency domains. For exploration at greater depths, natural source AEM systems are preferred because they are not limited by the strength of a transmitter. These methods operate in the frequency domain and by lowering the frequency, the depth of exploration can be increased. Ground exploration techniques can also be used to supplement AEM data. In particular, the MT method is used to map electrical resistivity contrasts and has a greater penetration depth than any AEM technique. Because ZTEM and MT are related as natural source techniques, it is straightforward to combine them in a joint inversion algorithm. Joint inversion of controlled and natural source methods is also routinely performed with data such as controlled source electromagnetic (CSEM) and MT (Mackie et al., 2007). The quantities that are measured by the ZTEM and MT techniques are briefly summarized below, followed by a short description of the e3dMTinv inversion algorithm developed at the University of British Columbia (Holtham and Oldenburg, 2010).

3.1 Theory

The MT method was first described by Tikhonov (1950) and Cagniard (1953), and measures a time series of three mutually perpendicular magnetic field components and two horizontal electric field components. The electric and magnetic fields are transformed into the frequency domain assuming a harmonic time dependence $e^{-i\omega t}$, where ω is angular frequency. These are used to calculate the impedance tensor $\boldsymbol{Z}$, which is defined as:

$$\begin{bmatrix} E_x(\omega) \\ E_y(\omega) \end{bmatrix} = \begin{bmatrix} Z_{xx}(\omega) & Z_{xy}(\omega) \\ Z_{yx}(\omega) & Z_{yy}(\omega) \end{bmatrix} \begin{bmatrix} H_x(\omega) \\ H_y(\omega) \end{bmatrix} \tag{1}$$

where the electric field *E*, the magnetic field *H*, and impedance $\boldsymbol{Z}$ are complex functions of the angular frequency ω. The impedance contains information about the electrical resistivity of the Earth. The penetration depth of an EM signal is a function of its frequency and the resistivity of the subsurface:

$$\delta \approx 503 \sqrt{\frac{\rho}{f}} \tag{2}$$

where δ is the penetration depth in meters, f is the signal frequency in Hz, and ρ is the resistivity in Ω·m of a homogeneous halfspace. ρ_a is the apparent resistivity and can be computed from the measured impedance $\boldsymbol{Z}$ by the following:

$$\rho_{xy}(\omega) = \frac{1}{\omega\mu_0} \left| \frac{E_x(\omega)}{H_y(\omega)} \right|^2 \tag{3}$$

where ρ_a has been written explicitly for the *xy* polarization.

Airborne ZTEM surveys do not measure the electric fields. Instead, the three magnetic field components are used to calculate the vertical magnetic field transfer function, or the tipper:

$$H_z(r) = [T_{zx}(r, r_0) \quad T_{zy}(r, r_0)] \begin{bmatrix} H_x(r_0) \\ H_y(r_0) \end{bmatrix} \tag{4}$$

where T_{zx} and T_{zy} are the tipper components derived from each polarization of the horizontal magnetic field. Note that the H_z component is a function of the receiver location r, whereas the H_x and H_y components are measured at the base station location, r_0. Like the impedance, the tipper components are complex functions of angular frequency. Note that the tipper will be zero over the center of a conductive body, as the vertical magnetic field component changes sign at this location. This means that tipper measurements are sensitive to lateral resistivity variations, including resistivity structures not directly below the observation point. Tipper data can also be collected at an MT station by measuring H_x, H_y, and H_z with three magnetic field channels. Unlike Equation 4, the three magnetic field components in MT are usually measured at the same location.

3.2 Inversion Algorithm

The ZTEM and MT data were inverted using the UBC GIF e3dMTinv code to produce a resistivity model of the Earth. This algorithm was adapted by Holtham and Oldenburg (2010) for ZTEM inversion and was an extension of the MT inversion algorithm developed by Farquharson et al. (2002). The inversion uses a Gauss-Newton algorithm variant that seeks to minimize the objective function Φ which consists of two terms: (1) the misfit between observed and predicted data ϕ_d, and (2) a model norm ϕ_m that quantifies the resistivity model properties:

$$\Phi = \phi_d + \beta\phi_m \tag{5}$$

where β is the regularization parameter that is gradually decreased with each iteration until the desired misfit is achieved. The measure of data misfit ϕ_d is the sum of squares weighted by the data uncertainty:

$$\phi_d = \|\boldsymbol{W_d}(\boldsymbol{d}^{obs} - \boldsymbol{d}^{pred})\|_2^2 \tag{6}$$

where $\boldsymbol{d}^{obs}$ and $\boldsymbol{d}^{pred}$ are vectors containing the observed and model predicted data, respectively; $\boldsymbol{W_d}$ is a diagonal matrix containing the reciprocals of the data uncertainties, and $\|\cdot\|_2$ represents the l_2 norm. The model norm is defined as:

$$\phi_m = \sum_{k=1}^{4} \alpha_k \left\|\boldsymbol{W}_k(\boldsymbol{m} - \boldsymbol{m}^{ref})\right\|_2^2 \tag{7}$$

where $\boldsymbol{W}_1$ is a diagonal matrix, and $\boldsymbol{W}_2$, $\boldsymbol{W}_3$, and $\boldsymbol{W}_4$ are the first order finite-difference matrices for the x, y, and z directions, respectively. The vectors $\boldsymbol{m}$ and $\boldsymbol{m}^{ref}$ contain the logarithmic cell conductivities of the recovered and reference model, respectively. The factor α_1 (or α_s) controls the closeness of the inversion model to the reference model, and $\alpha_{2,3,4}$ (or $\alpha_{x,y,z}$) control the spatial smoothing in the x, y, and z directions.

The inversion algorithm used for the joint inversions is the same as that used for the single inversions of the ZTEM and MT data. However, the data misfit term differs for the joint inversion approach to accommodate both data sets. As in Equation 5, the objective function Φ is still dependent on the data misfit and model regularization, except ϕ_d is the sum of the MT and ZTEM data misfits, ϕ_d^{MT} and ϕ_d^{ZTEM}. In most cases the number of data points in the ZTEM survey will be much greater than the number of data points from the MT survey. For example an MT survey with 20 stations recording the full impedance tensor (8 components) at 10 frequencies will have 1,600 total data points. A similar scale ZTEM survey with fifteen 10 km flight lines measuring approximately every 10 m will have 300,000 data points (4 tipper components at 5 frequencies). Without compensating for over one hundred times as many ZTEM data points as MT data points, it is easy for the inversion to overfit the ZTEM data. Even if the inversion reaches the desired root-mean-square (r.m.s.) misfit, the resulting resistivity model may predominantly contain structure required by the ZTEM data. The data misfit terms for ZTEM and MT must be balanced so that they equally influence the overall data misfit function. Following the method of Holtham (2012), the total data misfit ϕ_d was modified from Equation 6:

$$\phi_d = \left|\boldsymbol{W}_{d1}\left(\boldsymbol{d}_{ZTEM}^{obs} - \boldsymbol{d}_{ZTEM}^{pred}\right)\right\|_2^2 + \gamma\left|\boldsymbol{W}_{d2}\left(\boldsymbol{d}_{MT}^{obs} - \boldsymbol{d}_{MT}^{pred}\right)\right\|_2^2 \tag{8}$$

where γ is the data weighting term, and $\boldsymbol{W}_{d1}$ and $\boldsymbol{W}_{d2}$ are diagonal matrices whose elements are the reciprocals of the ZTEM and MT data uncertainties, respectively. The vector $\boldsymbol{d}^{obs}$ contains the observed data and $\boldsymbol{d}^{pred}$ the model predicted data.

The weighting factor γ allows both datasets to be equally weighted without having to downsample the data. In order for both datasets to equally influence the inversion, γ should be equal to the ratio of the number of ZTEM data, N_{ZTEM}, divided by the number of MT data, N_{MT}. This effectively increases the influence of the MT data misfit in the misfit function by forcing the inversion to more closely fit the fewer MT data points. The optimal γ value must be determined through trial inversions, because the number of data points is not the only factor that influences the data weighting. If the two datasets have different spatial sampling, then a given subset of the model is influenced by a different number of ZTEM and MT data. The weighting can also be defined for each frequency. For example, different weights can be assigned to the frequencies that overlap in the two datasets and the ones that do not. These methods of weighting were not explored in this study but could prove to be useful in certain situations.

4. Geology and Previous Geophysical Exploration of the Morrison Deposit

This case study focuses on the Morrison porphyry Cu-Au-Mo deposit, currently being developed by Pacific-Booker Minerals Inc. The deposit is located in the northern Babine Lake region of British Columbia, Canada, which is well known for previously mined porphyry Cu deposits at Bell (77.2 Mt, 0.48% Cu) and Granisle (52.7 Mt, 0.43% Cu) (Robertson, 2009). The

Morrison deposit has a measured and indicated resource of 207 Mt at 0.39% Cu, and is in the advanced stage of development (Robertson, 2009).

The Morrison deposit is located in the Stikinia Terrane, which is a former island arc that was accreted to North America in the middle Jurassic, along with several other island arc terranes (Monger and Price, 2002; Nelson and Colpron, 2007). After accretion, the Stikinia terrane experienced deposition of volcanic and sedimentary rocks in the Babine Lake area, including the Middle-Late Jurassic Bowser Lake Group. Porphyry deposit formation occurred when these Mesozoic age volcanic and sedimentary rocks were intruded from the Late Cretaceous to early Cenozoic (McMillan et al., 1995). This includes the Morrison porphyry deposit which is associated with the Eocene Babine Lake igneous suite.

As illustrated in Figure 3, the Morrison deposit is genetically and spatially related to an Eocene biotite-feldspar porphyry stock (BFP), which intruded into the Middle-Late Jurassic Bowser Lake Group sediments at 52.54 ± 1.05 Ma (Liu et al., 2016). The Eocene intrusive rocks consist of a main circular stock and a series of thin, elongate dikes. The host rock lies in the northwest trending Morrison Graben, which contains a down-faulted block of Lower to Middle Jurassic Hazelton Group volcanic and sedimentary rocks. The Morrison Graben contains a pair of smaller north-northwest-trending faults (F1 and F2 in Figure 3B). F2 is a north trending dextral strike-slip fault that bisects the main BFP stock with an offset of about 300 m (Simpson, 2007).

Potassic alteration at Morrison is mainly found within the central BFP stock. Cu mineralization occurs as vein-hosted and disseminated chalcopyrite and bornite, with minor molybdenite (dated at 52.54 ± 0.22 and 53.06 ± 0.22 Ma; Liu et al., 2016). Two semicircular copper zones with an average grade of 0.39% Cu are surrounded by pyrite halos related to propylitic (chlorite-carbonate) alteration, and are offset to the northwest and southeast by the fault F2 (Figure 3). Although pyrite is usually associated with phyllic alteration, little phyllic alteration has been observed at Morrison. Argillic alteration (clay and carbonate minerals) occurs in association with the F2 fault, and overprints other alteration types (Robertson, 2009; Liu et al., 2016).

The first geophysical work performed at Morrison consisted of ground IP and magnetic surveys performed by Peter E. Walcott & Associates Ltd. in 2000 (Walcott, 2001). The results were used to define the spatial extent of mineralized zones. An airborne AeroTEM time domain survey was then carried out in late 2008 as part of a larger project for Geoscience BC (Aeroquest Surveys, 2009).

In May 2010 Geotech Ltd. carried out a ZTEM survey over the Morrison property. Fifteen 10.9 km lines were flown with a line spacing of 250 m (Figure 3). The survey was flown with flight lines perpendicular to the predominant geological strike with the x-direction aligned to N50°E. The processed frequency band consisted of five frequencies: 360, 180, 90, 45, and 30 Hz. The airborne receiver coil measured the vertical component of the magnetic field, and was towed from a helicopter with an average ground clearance of 80 m. The base station receiver consisted of two orthogonal coils to measure the magnetic fields in the x and y-directions corresponding to N50°E and N40°W, respectively. Assuming the magnetic fields used in ZTEM are spatially and temporally coherent over large distances the precise location of the base station is not important, so long as it is close enough (5 – 20 km) to measure horizontal magnetic fields that are coherent with those in the survey area (Holtham and Oldenburg, 2010).

To compare the airborne ZTEM tipper data to conventional ground-based measurements, an MT survey was completed over the Morrison deposit in July 2013 by a team from the University of Alberta with the assistance of Peter E. Walcott & Associates Ltd. MT data were collected in the frequency band 300 - 0.001 Hz with Phoenix Geophysics V5-2000 instruments and magnetic induction coils at a total of 37 stations. The station spacing was approximately 500 m over the deposit and increased to 1 km around the deposit to provide a regional constraint for the 3-D inversion (Figure 3). Vertical magnetic fields were measured at each MT station to allow comparison to the previously acquired ZTEM data. The MT data acquisition area was limited by available road access and terrain, and as a result the MT survey area was not as spatially extensive as the airborne ZTEM survey. In particular the northeastern portion of the ZTEM survey was not sampled by any MT stations. The MT survey grid was not as uniform as the ZTEM survey because the presence of Morrison Lake to the west of the Morrison Graben prohibited the collection of ground MT data in this area.

Topography can have an effect on the tipper data since there is a large resistivity difference between the earth and air. The topography at the Morrison deposit varies from about 800 m to 1400 m in the ZTEM survey area. The topographic effect was quantified by calculating the predicted ZTEM data over a uniform earth with resistivity of 500 Ωm (i.e. no resistivity variations below ground) at a frequency of 360 Hz (Figure 4). Some of the predicted data are the same order of magnitude as the measured data, which means topography alone can significantly influence the measured ZTEM data. This shows that it is important in the inversion to include model cells at the surface small enough to accurately replicate the air-earth interface. The topographic response is not as significant at lower frequencies such as 30 Hz because the skin depth is larger compared to the scale of topographic changes.

The ZTEM and MT datasets should exhibit similar features because both surveys measured tipper data in the same area. The observed tipper data at each MT station location were compared to the tipper data from the closest ZTEM recording location (Figure 5). There is good correlation between the airborne and ground tipper at the overlapping frequencies between 360 - 30 Hz. The two datasets can also be displayed as induction arrows as in Figure 6. These arrows are plotted using the real T_{zx} and T_{zy} components and in this convention point toward conductors (Parkinson, 1959). The induction arrows at the Morrison deposit consistently point toward the southwest for frequencies of 30 Hz and 28 Hz for the ZTEM and MT data, respectively. The agreement is similar to that reported by Hübert et al. (2015) at the Newton deposit.

Although MT tipper data correlate well with the ZTEM tipper data, the MT tipper data were not inverted in this study. It should be noted that including the MT tipper data would have provided a wider frequency band and thus more sensitivity to deep structure. However, to simplify the joint inversion procedure and interpretation we will only show the simple case of ZTEM tipper and MT impedance. While comparison of the ZTEM and MT tipper data in individual and joint inversions will make an interesting future study, it is not the goal of this paper.

5. Separate inversions of the Morrison ZTEM and MT data

The ZTEM tipper and MT impedance data were first inverted separately. The ZTEM data at five frequencies from 360 – 30 Hz were inverted and because no error estimates were provided with the data, the error level was set to 0.01. The same mesh with a minimum cell size of 75 m x 75 m was used for the ZTEM, MT and joint inversions, and the initial resistivity model was a 500 Ωm halfspace. It should be emphasized that the ZTEM inversion must start with a reasonable estimate of background resistivity in order to recover accurate resistivity values in the model. For example, the background resistivity can be determined from MT impedance data because they contain information about the absolute resistivity values. Several test ZTEM and MT inversions were run with starting resistivity values from 50 – 1000 Ωm. The 500 Ωm inversions converged quickly and had the lowest final misfits, so this value was chosen as the starting and background resistivity. The ZTEM inversion converged to an r.m.s. misfit of 0.91, with excellent data fit along each flight line. An example of the observed and predicted data at 90 Hz is shown in Figure 7.

The inverted MT data consisted of twelve frequencies from 132 – 0.7 Hz. Although the highest frequency of the data was 320 Hz, the first few data points (highest frequencies) were biased downward or too noisy for inversion. The inversion error floor was set to 7.5% of Z_{xy} applied to Z_{xy} and Z_{xx}, and 7.5% of Z_{yx} applied to Z_{yx} and Z_{yy}. The measured diagonal impedance components are often several orders of magnitude smaller than the off-diagonal components for a 1-D or 2-D resistivity structure. However, the diagonal impedance components at Morrison were relatively large and only one order of magnitude smaller than the off-diagonal components. This is an indication of a 3-D resistivity structure and unfortunately the inversion was unable to fit distortion at several stations. Four stations were not used in the final inversion due to poor data quality or low amounts of signal in the relevant frequency bands. In addition five stations displaying a large static shift (2 orders of magnitude or greater) were not used because the inversion was not able to fit these data. Finally, five stations with large impedance phase splits or out-of-quadrant phases did not adequately fit the data and were excluded from the final inversion. Static shifts and out-of-quadrant phases are specific cases of distortion of the MT impedance data generally due to small 3-D structures with a spatial scale less than the minimum skin depth, and structures outside of the survey area that cause current channeling. One strategy to account for static shifts in 3-D inversion is to finely discretize the uppermost region of the model. This allows small-scale distorting features to be included in the resistivity model. However, the stations with the most severe static shifts were still not adequately fit by the inversion algorithm. In addition, the distortion due to current channeling requires further analysis and is not included in this paper. A total of 23 MT stations were used in the final inversion. These are shown as black circles in Figure 3A.

The starting model for the first MT inversion was a 500 Ωm halfspace. There is good agreement between the observed MT data and the predicted model responses. The final r.m.s misfit was 0.91 and the data fit was inspected at each station and frequency to ensure consistency. A sample of the data fit for each station at a frequency of 8.1 Hz is shown in Figure

8. Even the diagonal components (*xx* and *yy*), which tend to be noisier than the off-diagonal components, are fit well at most frequencies.

The resistivity models computed from the ZTEM and MT inversions are briefly compared here, but are discussed in more detail in Section 7. Figure 9 shows horizontal slices of the ZTEM, MT, and joint inversion models at five depths: 633 m, 483 m, 333 m, -417 m, and -1017 m elevation above sea level. For reference, the elevation at the Morrison deposit is about 800 m above sea level. At 633 m and 483 m elevation the MT model contains more small-scale resistivity features around the deposit (Figures 9B and 9E) than the ZTEM model (9A and 9D). One explanation for this is the different model regularization in each inversion due to the large difference in the amount of ZTEM and MT data. In addition, these small-scale features are required by the MT inversion because some stations experience distortion from small conductive structures when measuring electric field data. Both the MT and ZTEM models contain the shallow conductor C1 to the southwest of the deposit and the resistive feature R1 to the east of the deposit. One major difference between the two models lies to the southwest of the deposit. In the ZTEM model C1 is bordered by the western edge of the Morrison Graben at 633 m elevation, but in the MT model C1 is a smaller feature that does not reach the Morrison Graben. The MT model cannot resolve the eastern edge of C1 because the MT survey could not sample the area of Morrison Lake. This disparity is addressed in the following joint ZTEM-MT inversion. The resistive feature R2 and the moderately conductive C2 appear in both models. However, the resistivity values are more extreme in the MT inversion, with R2 more resistive and C2 more conductive than in the ZTEM inversion. The spatial extents of R1 and C2 are better constrained in the ZTEM model because there are no MT stations in the northeast portion of each panel. In addition, features to the northwest of the deposit were required by the MT data and are located outside the ZTEM survey area, and are poorly constrained in the ZTEM model. However, the data at the lowest frequencies are still sensitive to structure outside of the survey area. At elevations of -417 m and -1017 m the MT model contains the conductor C3, but the ZTEM model does not contain a highly conductive feature at these elevations. There is also a distinct conductor south of R1 in the ZTEM and MT models slices at 633 m, 483 m, and 333 m elevation (Figure 9). The location of this conductor agrees well with the location of the Hearne Hill deposit, which is associated with two breccia pipes 2 km southeast of the Morrison deposit (Simpson, 2007; Robertson, 2009).

Figure 10 shows vertical slices of the resistivity models on the profiles A-A’ and B-B’ (see Figure 9A for profile traces). Profile A-A’ intersects the Morrison deposit at an angle of N50°E and B-B’ intersects the deposit at an angle of N40°W. The slices along A-A’ clearly show that the horizontal geometry of C1 from 1.5 to 2.5 km along profile is different in the ZTEM and MT inversions. As seen in Figure 10C at about 3.5 km along profile, the MT resistivity model also contains a small, highly conductive body in the upper 100 m above the Morrison deposit. It should be noted that the A-A’ vertical slice is coincident with the 2-D inversion by Geotech Ltd. (2010) along the same profile, as shown in the Appendix. The 2-D ZTEM inversion detected a conductor that could be C3, whereas the 3-D ZTEM inversion did not. At about -500 m elevation the MT resistivity model contains the conductor C3 that is not imaged in the ZTEM resistivity model. This suggests that detection of this feature requires the use of a joint ZTEM-MT inversion. The fact that the MT inversion images C3 better than the ZTEM inversion is due to a number of reasons:

(1) The ZTEM data have a minimum frequency of 30 Hz, giving a skin depth of 2 km in a 500 Ωm halfspace. The presence of some low resistivity anomalies will reduce this value, placing C3 on the limit of detection with ZTEM data. In contrast, the MT inversion uses a minimum frequency of 0.7 Hz giving a skin depth of 13 km.

(2) The MT and ZTEM inversions are a trade-off between achieving data fit and finding a spatially smooth model. Different spatial regularizations can emphasis shallow or deeper structure.

In addition to comparing model slices side-by-side, cross-plots are a qualitative way to compare the electrical resistivities of two different models at the same location. If the resistivity values of individual model cells in both models were exactly the same, the plot would be a straight line with a slope of one. Figure 11 shows the correlation at progressively lower elevations in each panel (deeper horizontal sections). The resistivity value for each individual model cell was plotted (horizontal axis is MT model resistivities, vertical axis is the ZTEM model resistivities) and the cross-plots show that there is a correlation between the resistivity values in each model. The correlation is weaker near the surface due to small near-surface inhomogeneities in the MT resistivity model. At intermediate depths there is a good correlation in resistivity values between the two models. The correlation is not as strong below 425 m elevation.

6. Morrison Joint ZTEM-MT Inversion

The first step in the joint inversion was to determine a value of γ that would optimize the misfit of the ZTEM and MT data. Ten joint ZTEM-MT inversions were run using different values of γ to investigate the effect on the data misfits and models. From Equation 8 it is clear that increasing the weighting factor γ should increase the influence of the MT data in the joint inversion. As a result the r.m.s. misfit for the MT data should decrease for inversions using a larger γ. This trend is apparent from the joint inversions presented in Figure 12. For the lowest weighting factor tested, γ = 0.1, the MT data r.m.s. misfit is much higher than the ZTEM data r.m.s. misfit. In contrast, when γ = 50, the ZTEM r.m.s. misfit is larger than the MT r.m.s. misfit. In this case the ZTEM data fit is suffering from the inversion putting too much weight on the MT data. To achieve a balance between the two data misfits, we chose γ = 3 as the preferred weighting factor because in this inversion the final misfits of the ZTEM (0.98) and MT (0.93) data are close to the total misfit of 0.98. The observed and calculated data from this inversion are shown in Figures 13 and 14 at a ZTEM frequency of 90 Hz and an MT frequency of 8.1 Hz. It should be noted that the curves of misfit values in Figure 12 are not perfectly smooth because each inversion ended after a different number of iterations. The number of β iterations needed for each inversion was between 44 and 54. We considered an acceptable level of convergence if there was a very small (< 1%) change in misfit and the model structure did not change an appreciable amount in the final iterations. The exceptions are the joint inversions with γ = 30 and γ = 50. The r.m.s. misfit curves for these higher γ values did not monotonically decrease at later iterations. Though the reason for this was not further investigated, this may be a problem with the regularization. From Equation 8 a large γ may cause the value of ϕ_d to become large compared to ϕ_m, and a different starting value of β may be needed.

Cross-plots were used to analyze the effect of changing the data weighting. For example, a low weighting factor such as $\gamma = 0.1$ places less weight on fitting the MT data, and the final resistivity model should look similar to the model from the ZTEM inversion. We expect the opposite with a high weighting factor such as $\gamma = 50$: the resulting resistivity model should appear similar to the model obtained from an inversion of only MT data. Figure 15 shows the results from the two extreme cases of $\gamma = 0.1$ and $\gamma = 50$ and the preferred $\gamma = 3$. The horizontal slices from each model are at 425 m elevation. As expected, for $\gamma = 0.1$ there is a strong correlation in resistivity values between the ZTEM and joint resistivity models because the ZTEM data are highly weighted in the joint inversion. Figure 15D shows a weaker correlation between the MT inversion and the joint inversion with $\gamma = 0.1$. For $\gamma = 50$ there is a weaker correlation between the ZTEM and joint models than the MT and joint models. The cross-plots for $\gamma = 3$ show a more balanced level of correlation for the ZTEM and MT data in the joint inversion.

Figure 16 shows a vertical slice along profile A-A' through the ZTEM, MT, and joint inversion models. With $\gamma = 0.1$, the joint model greatly resembles the model from the ZTEM inversion. As the weighting factor γ increases, deeper features required by the MT data are included in the model. The models with the largest γ values resemble the model from the MT inversion. This demonstrates how the joint inversion is a trade-off between emphasizing the ZTEM and MT data. The joint model from $\gamma = 3$ clearly contains structure that is required by both datasets.

The joint resistivity model (Figures 9 and 10) contains most of the features seen in the ZTEM and MT resistivity models. C1 and R1 are present in all models to the southwest and northeast of the Morrison Graben, respectively. R2 extends to approximately 1 km below the surface and is flanked by two conductive bodies to the southwest and northeast (C2) that correlate with the bounding faults of the Morrison Graben. C2 appears as a conductive feature in all three models but is more conductive in the MT and joint models. As mentioned in the previous section, the ZTEM model at 633 m elevation images C1 as a continuous feature to the edge of the Morrison Graben, but the MT model does not (Figures 9A and 9B). This disparity is simply due to the limited spatial sampling of the MT survey. The joint ZTEM-MT model at 633 m elevation is a clear improvement on the MT model since C1 is imaged to the same spatial extent as in the ZTEM model. C3 is a highly conductive feature in the MT and joint inversions that is not as clearly imaged in the ZTEM inversion. The Appendix includes a resolution test indicating that C3 is a feature that is required by the lower frequency MT data (Figure A2). Combined with the improved spatial resolution of the ZTEM data, it is clear that the primary strength of each dataset has a positive impact on the joint resistivity model.

7. Discussion

The ZTEM, MT, and joint ZTEM-MT models contain similar resistivity features that can be correlated with the deposit lithology, hydrothermal alteration zones, and sulfide mineralization. The features from the inversions and additional geophysical studies are considered in two categories: lithologic and alteration related (Table 1). The joint inversion was chosen as the preferred model for interpretation because it represents a balance between the advantages of each data type. The joint inversion model, which contains features from the ZTEM and MT models, is first compared to late-time tau and then to the magnetic susceptibility data from an AeroTEM airborne survey (Aeroquest Surveys, 2009).

7.1 AeroTEM Late-time Tau

In TDEM surveys, a transmitter induces electric currents in the Earth and the decaying magnetic field is measured as a function of time (Nabighian and Macnae, 1991). Maps of the decay constant (tau) show which areas are relatively conductive (i.e., current flows for a longer time, with higher tau values) or relatively resistive (lower tau values). It is important to note that the sampling depth of a TDEM survey depends on the resistivity of the subsurface. This is similar to the skin depth in frequency domain EM surveys. The TDEM sampling depth can be approximated in a halfspace as

$$\delta_T = \frac{1}{2.3}\sqrt{\frac{2\rho t}{\mu}} \tag{9}$$

where δ_T is the sampling depth, ρ is the resistivity of the halfspace, t is the measurement time of the secondary magnetic field, and μ is the magnetic permeability (Meju, 1996). For example, with a representative value of 400 μs for tau and a resistivity of 10 Ωm, and assuming the free space value of μ, the sampling depth δ_T is 35 m. In a more resistive environment where tau is 100 μs and the resistivity is 1000 Ωm, the sampling depth is 175 m.

Figure 17B shows the late time tau map from the AeroTEM survey over the Morrison deposit (Aeroquest Surveys, 2009). The higher tau values to the southwest of the Morrison deposit match well with the low resistivity feature C1 observed in the joint inversion model. This area coincides with the Quaternary glaciolacustrine sediments around and below Morrison Lake. Because C1 extends several hundreds of meters below the surface, it also likely represents the Ashman Formation sedimentary unit. The edge of C1 correlates very well with the western edge of the Morrison Graben, where there is a geologic contact between the conductive sediments and sedimentary rocks of C1 and the intrusive rocks within the graben. The low tau values to the northeast of the deposit correlate well with feature R1 in the joint inversion model, which matches the known location of the Hazelton Group volcanic rocks to the east of the Morrison Graben. Within the deposit, there is a low tau anomaly that covers the northwestern half of the main BFP stock and the three intrusive BFP dikes. This matches the location of R2 in the joint inversion model. In the southeast half of the central BFP stock, there is a slightly elevated tau (200 – 250 μs) that could be explained by a higher concentration of sulfides outside the potassic alteration zone. This feature also appears in the joint resistivity model (Figure 17A) as a small, shallow conductor coincident with the southeast half of the orebody. The high tau anomaly immediately south of R1 corresponds to the high-grade breccia pipes of the Hearne Hill deposit. Note that the conductive feature to the northwest of the deposit (Figure 17A) does not appear as a strong tau anomaly. This could be due to the choice of inversion regularization and the fact that the geometry of this feature is not well-resolved with only two MT stations nearby. C2 does not appear as a strong tau anomaly in late-time tau map.

7.2 Aeromagnetic Data

The magnetic response of a porphyry deposit is dominated by the spatial distribution of unaltered hydrothermal magnetite. The Morrison deposit is hosted by sedimentary rocks of the Bowser Lake Group, which should contain negligible amounts of magnetite. In contrast, fresh igneous rocks of the Eocene Babine Intrusions are likely to contain moderate amounts of primary igneous magnetite, and the potassic alteration zone of the porphyry system should also contain small amounts of hydrothermal magnetite; as such, both the intrusive rocks and potassic alteration zones should show positive magnetic susceptibility anomalies as observed in Figure 17C (high magnetic susceptibility is shown in blue). R2 in the ZTEM and MT inversion models also matches reasonably well with the magnetic highs for the intrusive dikes; however, the aeromagnetic map shows two distinct magnetic highs at the location of R2. In addition, the > 0.3% Cu zone appears as two circular magnetic highs associated with hydrothermal magnetite in the potassic alteration zone. Whereas the northwest half of the > 0.3% Cu zone is highly resistive in the joint inversion, the southeast half did not appear resistive in the joint inversion. This area could have a lower resistivity due to a larger concentration of sulfides, particularly pyrite in the 1 – 5 wt.% zone shown in Figure 3B. There is a clear lithologic contact to the east of the deposit between the magnetite-poor Ashman Formation sedimentary unit and the mafic volcanic rocks of the Hazelton Group.

7.3 Deposit Lithology

The main lithologies are well resolved by the joint ZTEM-MT inversion. Igneous rocks generally have higher resistivity because they lack interconnected fluids in pore space compared to sedimentary rocks. The presence of clay minerals in the Quaternary sediments also has a strong control on resistivity. The Hazelton Group volcanic sequence is represented by a prominent resistive feature R1 (> 1000 Ωm) in the ZTEM and MT models. The position of R1 (Figure 18) to the east of the Morrison Graben correlates well with the position of the Hazelton Group outcrop area shown in Figure 3. Because ZTEM tipper data sharply define conductive boundaries, this is a well defined feature in the ZTEM inversion and also appears in the MT impedance inversion. R1 extends about 1 km further to the northeast in the ZTEM inversion because the ZTEM survey area was larger than the MT area (Figure 10). In the MT model R1 is in the same position as the ZTEM model but the northeastern edge is not constrained due to a lack of MT stations (shaded area in Figure 10).

The Quaternary sediments to the southwest of the deposit appear as the large conductive zone C1 in the joint inversion model (Figure 9C). This is typical of recent glaciolacustrine deposits that have large amounts of fluid pore space (Palacky, 1988) and may also contain highly conductive clay minerals. C1 may also be partially due to the Ashman Formation sedimentary unit because it extends several hundred meters below the surface. The edge of this low resistivity zone correlates well with the western edge of the Morrison Graben. This represents the interface between the conductive Quaternary sediments and Ashman Formation sedimentary rocks outside the graben and the resistive Eocene Babine intrusions within the graben.

The MT and joint inversion models contain the deep feature C3 (Figure 10). C3 is required by the low frequency MT data as shown in the resolution test (Figure A2). One possible explanation for the deep conductor is that the bounding faults of the Morrison Graben become close enough to appear as a single conductive body at about -500 m elevation. This would depend on the dip of the graben walls, and the dashed lines in Figure 10 are only approximated from the surface geology. C3 could also represent a larger, regional fault that is a remnant of the Mesozoic island arc accretions that included the Stikinia terrane. The position of C3 in the horizontal model slices agrees with the north-northwest geologic strike of the Babine Lake region. Another possible explanation for C3 is the presence of a deeper sulfide-rich zone that immediately underlies the porphyry system. Due to the spatial extent of the MT survey, the geometry of C3 is not as constrained as the shallow anomalies. For example, in Figure 10C there are no MT stations to the east of 4.5 km where the eastern edge of C3 is a gradual transition back to the starting 500 ohm.m model. The actual edge of C3 can only be accurately resolved if there are MT stations located above either side of it. The western edge of C3 is also not well constrained by the MT data because of the gap in coverage above Morrison Lake. The shaded regions in Figure 10 represent these areas of "low resolution" where there is minimum data sensitivity. In addition, the resistivity and thickness of C3 cannot be uniquely determined by the MT data. This is a known limitation of the MT method because it is sensitive to the product of conductivity and thickness (conductance). Therefore the depth to the bottom of C3 is not resolved, especially because this depth may be at the penetration limit of the modeled MT frequencies. For these reasons the deeper part of C3 has also been labelled as an area of low resolution (Figure 10).

7.4 Electrical Resistivity Correlated to Hydrothermal Alteration and Mineralization

The alteration at Morrison is concentrically zoned over the main BFP intrusive stock. The central potassic core grades outward into a propylitic halo, with argillic alteration overprinting other alteration types. The feature R2 is likely the resistivity signature of the potassic core as well as the BFP intrusive dikes to the northwest of the deposit. The Morrison deposit is outlined in Figure 18B but does not appear as a strong resistivity anomaly in the joint inversion. The porphyry deposit model in Figure 1 predicts a higher resistivity at the deposit core associated with potassic alteration, but the inversions show that the highly resistive feature R2 is not only associated with the main BFP stock. One possibility is that the geometry of the intrusions shown in Figure 18A may be different than they appear at the surface.

The conductor C2 is a moderately conductive feature in the joint inversion model. It should be noted that the location of C2 also coincides with a small lake about 200 m north of the Morrison deposit. Even a small amount of clay or sediments at the lake could contribute to a shallow low resistivity feature in the model. C2 is outside the mapped pyrite halo so it is unlikely to be associated with a higher concentration of sulfides (Figure 18B). Even though C2 is spatially coincident with the eastern edge of the Morrison Graben, the joint resistivity model does not contain a continuous low resistivity feature along the eastern edge of the graben. This suggests that the low resistivity of C2 is not controlled by the graben.

The map in Figure 18B also compares the sulfide mineralization at Morrison with the joint ZTEM-MT resistivity model. The joint resistivity model matches well with the known geologic boundaries but there is a variable resistivity signature directly over the Morrison deposit. The 0.3 % Cu zone and the 1 – 5 % pyrite halo are not clearly defined in the resistivity model. There are conductive features on the order of a few hundred meters wide that match the location of the eastern pyrite halo. Looking at the depth slice in Figure 18B, the resistivity of the 0.3% Cu zone and the pyrite halo is about 50 – 300 Ωm, which is moderately resistive. Considering the main Cu ore body and particularly the pyrite halo contain the largest amount of sulfides, these areas should have a distinct resistivity response from the rest of the deposit. Using values from Figure 1, the 50 – 300 Ωm resistivity is on the upper end of the resistivity estimate for sulfide mineralization zones. From Figure 2, this resistivity range indicates that the sulfide mineralization at Morrison is mostly disseminated or in disconnected veins. This matches the type of mineralization at the Morrison deposit described by Simpson (2007), Robertson (2009), and Liu et al. (2016).

8. Conclusions

The ZTEM and MT methods were able to map the regional resistivity structure of the Morrison deposit. Depending on the exploration strategy at a particular deposit, this study suggests there is value in conducting a small-scale MT survey to integrate with the ZTEM data. Even though the ZTEM tipper data and MT impedance data were collected at different times and with different spatial sampling, the individual inversions resulted in similar resistivity models. The joint inversion of ZTEM and MT data yielded a resistivity model consistent with the local geology, but the sulfide mineralization in the 0.3% Cu zone and 1 – 5 wt.% was not clearly defined. However, the joint inversion is an improvement on the individual ZTEM and MT inversions. The main limitation of the ZTEM data was the lower skin depth compared to the MT inversion. The depth of the conductor C3 may have been close to the resolution limit of the

ZTEM data, resulting in a weakly imaged feature in the ZTEM inversion. The MT station spacing was limited by ground access so there were areas with limited resolution in the MT resistivity model. The joint inversion eliminated these shortcomings by combining the spatially dense sampling of the ZTEM dataset and the greater depth resolution of the MT data. However, from this study it is clear that for the MT data to be useful, a reasonable number of stations with a relatively uniform grid are needed. Additionally, we have shown that the joint inversion data fit and model structure must be inspected with several values of the weighting factor, γ. The individual ZTEM and MT data fits should be comparable in order to balance the contribution from each dataset.

Acknowledgements

This work was part of an NSERC-funded research collaboration between the University of Alberta, l'Université du Québec en Abitibi-Témiscamingue, the University of British Columbia, Amarc Resources Ltd., Geotech Ltd., and Gerald G. Carlson and John A. Chapman. We thank Geotech Ltd. for the ZTEM data and 2-D models, and Pacific Booker Minerals Inc. for access to their property. Peter E. Walcott & Associates Ltd., Paulina Hauf, Bahman Abbassi, and Lijuan Liu are thanked for in-field assistance. Thanks to Li Zhen Cheng for helpful discussions and to Doug Oldenburg and Roman Shekhtman for help with using the UBC inversion code. This research was enabled in part by support from WestGrid and Compute Canada. We thank the two anonymous reviewers for their suggestions that improved this paper.

References

Aeroquest Surveys (2009). Report on a helicopter-borne AeroTEM system electromagnetic & magnetic survey. Geoscience BC Technical Report.

BC Geological Survey (2006): MapPlace GIS internet mapping system; *British Columbia Ministry of Energy, Mines and Petroleum Resources*, MapPlace website, URL <http://www.MapPlace.ca>; [Jan, 2016].

Commer, M., and Newman, G. A. (2009). Three-dimensional controlled-source electromagnetic and magnetotelluric joint inversion. *Geophys. J. Int.*, 178, 1305-1316.

Cooke, D.R., Hollings, P., and Walshe, J.L. (2005) Giant porphyry deposits: characteristics, distribution, and tectonic controls. *Economic Geology* 100, 801–818.

Farquharson, C.G., Oldenburg, D. W., Haber, E., and Shekhtman, R. (2002). An algorithm for the three-dimensional inversion of magnetotelluric data. Proceedings of the 72nd Annual International Meeting, *SEG Expanded Abstracts*, 649-652.

Geotech Ltd. (2010). ZTEM Tipper AFMAG Results over the Morrison Copper/Gold Porphyry deposit. Geotech Ltd. Technical Report, <http://geotech.ca/papers/ztem-tipper-afmag-results-over-the-morrison-coppergold-porphyry-deposit/>.

Holliday, J. R., & Cooke, D. R. (2007). Advances in geological models and exploration methods for copper±gold porphyry deposits. *Proceedings of Exploration* 7, 791-809.

Holtham, E. M. (2012). 3D Inversion of Natural Source Electromagnetic Data. Unpublished Ph.D. Thesis, The University of British Columbia, Vancouver, Canada, 137 p.

Holtham, E., & Oldenburg, D. W. (2010). Three-dimensional inversion of ZTEM data. *Geophysical Journal International* 182, (1), 168-182.

Hübert, J., Lee, B.M., Liu, L., Unsworth, M.J., Richards, J.P., Abbassi, B., Cheng, L.Z., Oldenburg, D.W., Legault, J.M. and Rebagliati, M. (2015). Three-dimensional imaging of a Ag-Au-rich epithermal system in British Columbia, Canada, using airborne z-axis tipper electromagnetic and ground-based magnetotelluric data. *Geophysics* 81, (1), B1-B12.

Kaminski, V., Legault, J.M., and Kumar, H. (2010). The Drybones Kimberlite: a case study of VTEM and ZTEM airborne EM results. *Aust Soc Explor Geophys Ext Abstr*

Legault, J. M. (2015). Airborne Electromagnetic Systems- State of the Art and Future Directions. CSEG Recorder 40, (6), 38-49.

Legault, J. M., Wijns, C., Izarra, C., and Plastow, G. (2016). The Balboa ZTEM Cu-Mo-Au Porphyry Discovery at Cobre Panama. *ASEG Extended Abstracts*, 2016(1), 1-6.

Liu, L., Richards, J. P., Creaser, R. A., DuFrane, S. A., Muehlenbachs, K., and Larson, P. B. (2016). Geology and age of the Morrison porphyry Cu-Au-Mo deposit, Babine Lake area, British Columbia. *Canadian Journal of Earth Sciences*, published on the web 13 Apr. 2016.

Lo, B., and Zang, M. (2008). Numerical modeling of Z-TEM (airborne AFMAG) responses to guide exploration strategies, *SEG Technical Program Expanded Abstracts* 27, (1), 1098–1102.

Lowell, J.D., and Guilbert, J.M. (1970). Lateral and vertical alteration-mineralization zoning in porphyry copper ore deposits. *Economic Geology* 65, 373–408.

MacIntyre, D.G., Villeneuve, M.E., and Schiarizza, P. (2001). Timing and tectonic setting of Stikine Terrane magmatism, Babine-Takla lakes area, central British Columbia. *Canadian Journal of Earth Sciences* 38, 579–601.

Mackie, R. M., Watts, M. D., and Rodi, W. (2007). Joint 3D inversion of marine CSEM and MT data. *SEG Technical Program Expanded Abstracts* 26, 574-578.

McMillan, W.J., Thompson, J.F.H., Hart, C.J.R., and Johnston, S.T. (1995). Regional geological and tectonic setting of porphyry deposits in British Columbia and Yukon Territory, in Porphyry deposits of the northwestern Cordillera of North America, *Canadian Institute of Mining, Metallurgy and Petroleum Special Volume* 46, 40-57.

Meju, M. A. (1996). Joint inversion of TEM and distorted MT soundings: Some effective practical considerations. *Geophysics* 61, (1), 56-65.

Mitchinson, D. E., Enkin, R. J., and Hart, C. J. R. (2013). Linking Porphyry Deposit Geology to Geophysics via Physical Properties: Adding Value to Geoscience BC Geophysical Data. Geoscience BC Report 2013-14.

Monger, J., and Price, R. (2002). The Canadian Cordillera: Geology and Tectonic Evolution. CSEG Recorder Feb. 2002, 17–36.

Nabighian, M. N., and Macnae, J. C. (1991). Time domain electromagnetic prospecting methods. *Electrical methods in applied geophysics* 2, (part A), 427-509.

Nelson, J., and Colpron, M. (2007). Tectonics and metallogeny of the British Columbia, Yukon and Alaskan Cordillera, 1.8 Ga to the present. Mineral deposits of Canada: a synthesis of major deposit-types, district metallogeny, the evolution of geological provinces, and exploration methods: Geological Association of Canada, Mineral Deposits Division, Special Publication 5, 755-791.

Nelson, P. H., & Van Voorhis, G. D. (1983). Estimation of sulfide content from induced polarization data. *Geophysics* 48, (1), 62-75.

Orta, M., Legault, J. M., Prikhodko, A., Plastow, G., Zhao, S., and Ulansky, C. (2013). Passive and active helicopter EM survey comparisons over the 501 Project Cu-Zn volcanogenic massive sulphide at McFauld's Lake, northern Ontario. *ASEG Extended Abstracts* 2013, (1) 1-4.

Palacky, G. J. (1988). Resistivity characteristics of geologic targets. *Electromagnetic methods in applied geophysics* 1, 53-129.

Paré, P., and Legault, J. M. (2010). Ground IP-Resistivity and Airborne Spectrem and Helicopter ZTEM Survey Results Over Pebble Copper-moly-gold Porphyry Deposit Alaska. *SEG Annual Meeting Expanded Abstracts* 29, 1734-1738.

Pare, P., Gribenko, A.V., Cox, L.H., Čuma, M., Wilson, G.A., Zhdanov, M.S., Legault, J., Smit, J. and Polome, L. (2012). 3D inversion of SPECTREM and ZTEM airborne electromagnetic data from the Pebble Cu–Au–Mo porphyry deposit, Alaska. *Exploration Geophysics* 43, (2), 104-115.

Parkinson, W. D. (1959). The influence of continents and oceans on geomagnetic variations. *Geophys. J. R. astr. Soc*., 6, 441-449.

Richards, J.P. (2003) Tectono-magmatic precursors for porphyry Cu-(Mo-Au) deposit formation. *Economic Geology* 98, 1515–1533.

Richards, J. P. (2009). Postsubduction porphyry Cu-Au and epithermal Au deposits: Products of remelting of subduction-modified lithosphere. *Geology* 37**, (**3), 247-250.

Richards, J. P. (2011). Magmatic to hydrothermal metal fluxes in convergent and collided margins. *Ore Geology Reviews* 40, 1-26.

Robertson, J. (2009). Morrison Copper/Gold Project – Feasibility Study: NI43-101 Report.

Sasaki, Y., Yi, M. J., and Choi, J. (2014). 2D and 3D separate and joint inversion of airborne ZTEM and ground AMT data: Synthetic model studies. *Journal of Applied Geophysics* 104**,** 149-155.

Sattel, D., & Witherly, K. (2015). The 3D joint inversion of MT and ZTEM data. *ASEG Extended Abstracts* 2015, (1), 1-4.

Seigel, H.O., Nabighian, M., Parasnis, D.S. and Vozoff, K. (2007). The early history of the induced polarization method. *Leading Edge* 26, 312–321.

Sillitoe, R.H. (1972). A plate tectonic model for the origin of porphyry copper deposits. *Economic Geology* 67, 184–197.

Sillitoe, R.H. (1973). The tops and bottoms of porphyry copper deposits. *Economic Geology* 68, 799–815.

Sillitoe, R. H. (2010). Porphyry copper systems. *Economic Geology* 105, (1), 3-41.

Simpson, R.G. (2007). Mineral resource update: Morrison project. Pacific Booker Minerals Inc., 66 p.

Walcott, P. E. (2001). A geophysical report on Magnetic and IP Surveying, Morrison Property.

Wannamaker, P. E., and Legault, J. M. (2014). Two-Dimensional Joint Inversion Of ZTEM And MT Plane-Wave EM Data For Near Surface Applications. *27th Annual Symposium on the Application of Geophysics to Engineering and Environmental Problems (SAGEEP).*

Ward, S. H. (1959). AFMAG-airborne and ground. *Geophysics* 24, (4), 761-787.

Appendix

A set of 2-D ZTEM inversions performed by Geotech Ltd. (2010) suggest that the ZTEM data do have some sensitivity to C3 because the models contain a conductor at the same depth and location as C3 (Figure A1). The 3-D ZTEM model contains only a moderately conductive feature at this depth.

A sensitivity test was performed to assess if C3 was a feature required by the low frequency MT data. An iteration of the joint inversion was selected when the misfit started to converge to its final value, and C3 was replaced by the background 500 Ωm resistivity (Figure A2). The inversion was restarted using this edited model as the starting model and the reference model. C3 re-appeared at the same depth and location after nine iterations, which suggests that C3 is a feature required by the MT data. The presence of C3 in the joint inversion model demonstrates the contribution from the lower frequency MT data. Note that the ZTEM model does contain a feature with moderate resistivity (300 Ωm) between -500 m and -1km elevation that may be related to C3.

Figures and table with captions

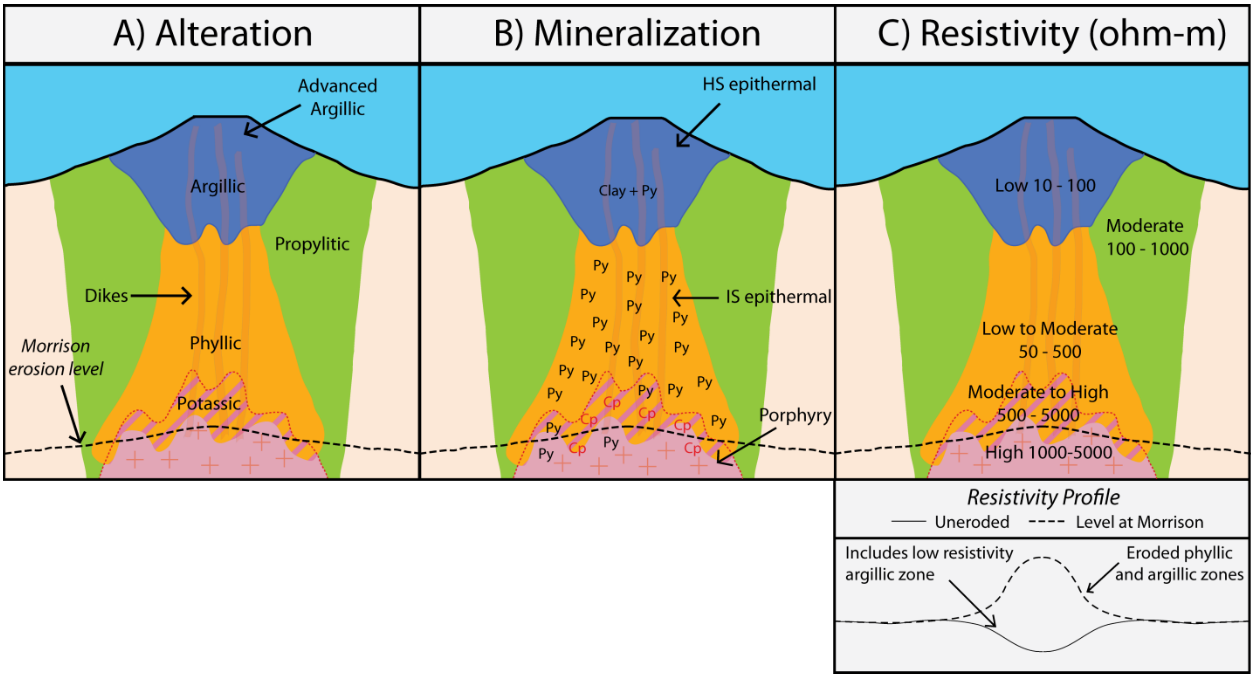

Figure 1: Alteration, mineralization and expected electrical resistivity responses for uneroded and eroded porphyry deposits. (A): Typical porphyry system alteration pattern. The dashed line represents the approximate erosion level of the Morrison deposit. (B): Expected sulfide mineralization, note the pyrite enrichment outside of the potassic core. (C): Electrical resistivity of alteration zones. The lower panel shows the expected responses for an uneroded and eroded porphyry deposit. Py = pyrite, Cp = chalcopyrite. Modified from Hübert et al. (2015).

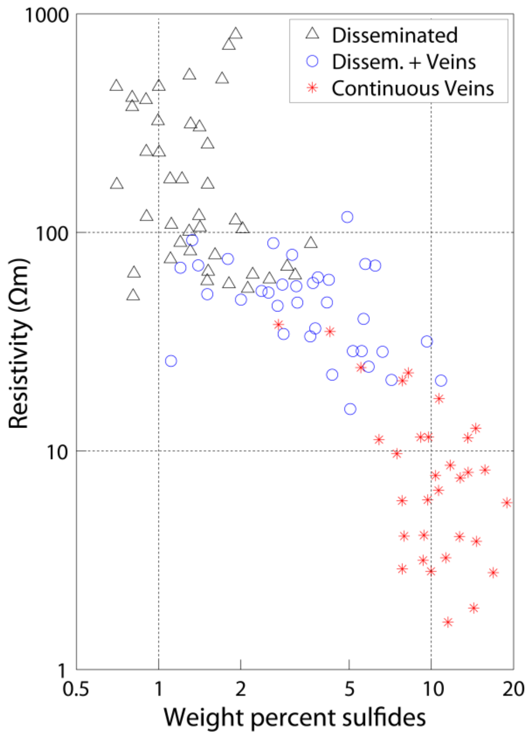

Figure 2: Relationship between sulfide weight percentage and electrical resistivity based on 109 in-situ measurements at porphyry deposits by Nelson and Van Voorhis (1983). For disseminated or discontinuous veins (< 3% wt.) the resistivity tends to be high and variable. As interconnectivity increases, there is a more direct relationship between increasing sulfide weight percent and decreasing resistivity. Modified from Nelson and Van Voorhis (1983).

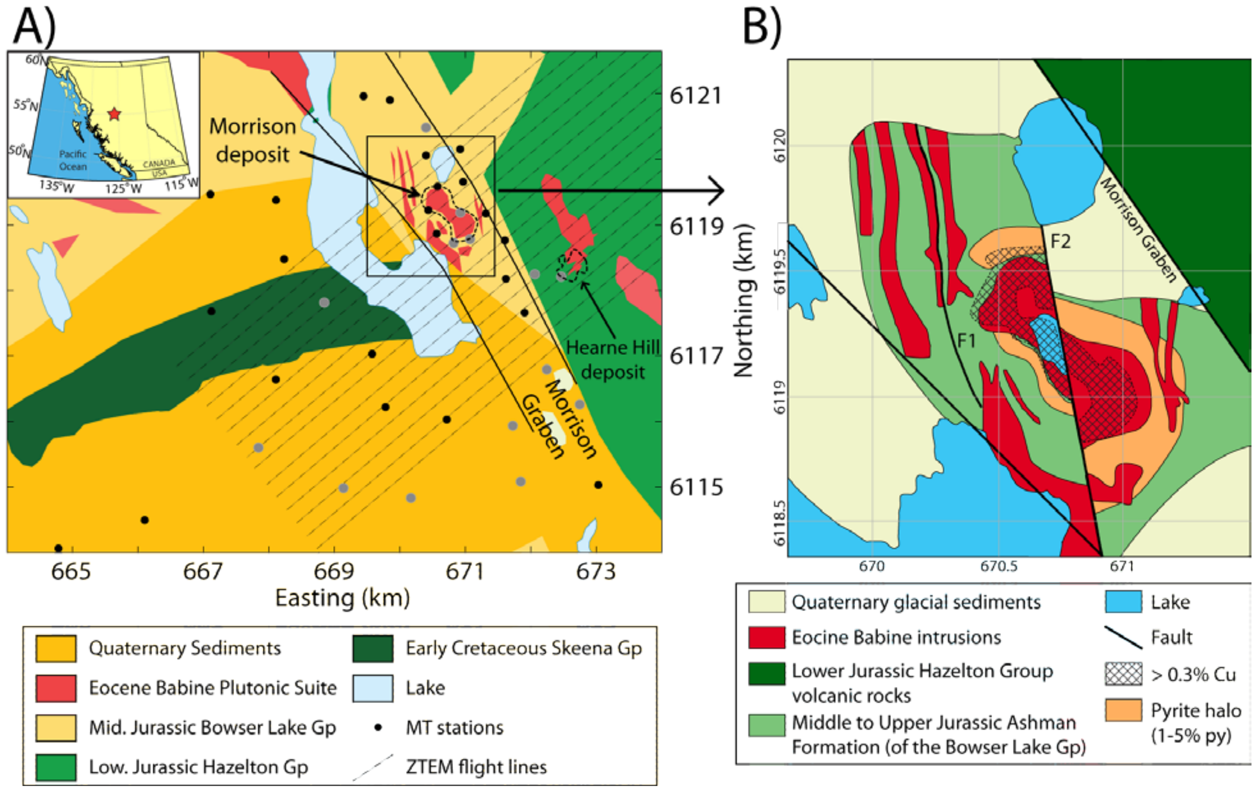

Figure 3: (A) Geologic map of the Morrison deposit with locations of the ZTEM survey (black lines) and MT survey (dark circles). Black stations are included in the MT and joint inversions. (B) The deposit area in detail. Adapted from BC Geological Survey (2006) and Liu et al. (2016). UTM grid in 1000 m units.

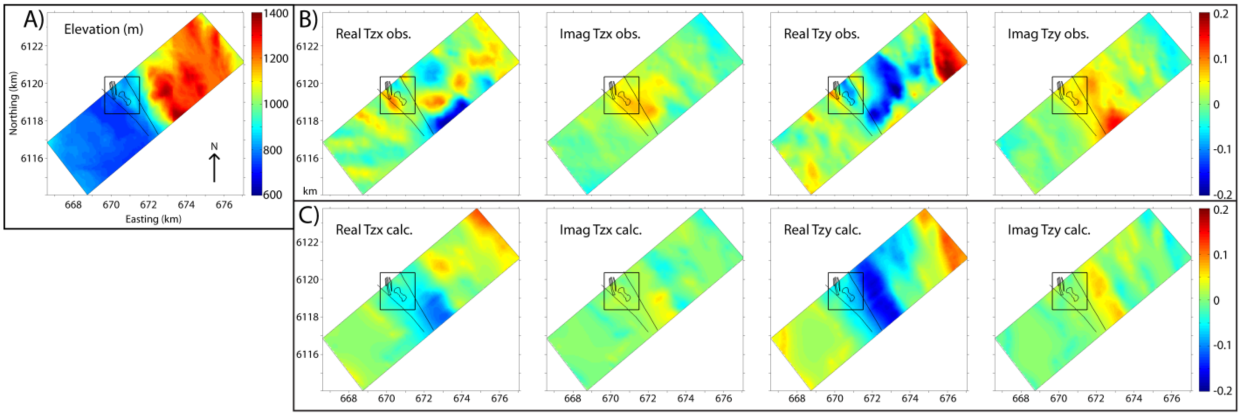

Figure 4: Effect of topography on the ZTEM data at a frequency of 360 Hz. (A) topography from the digital elevation model shows there is about 600 m of variation in elevation in the ZTEM survey area. (B) measured data due to both topography and sub-surface resistivity contrasts, (C) computed response of 500 Ωm halfspace with topography from (A). Note that predicted tipper data in (C) are the same order of magnitude as measured data in (B), suggesting that topography around the Morrison deposit has a large contribution to the observed tipper data. The Morrison orebody and 3 biotite-feldspar porphyry dikes are outlined in black, along with the bounding faults of the Morrison Graben. Black box is the deposit area shown in Figure 3B.

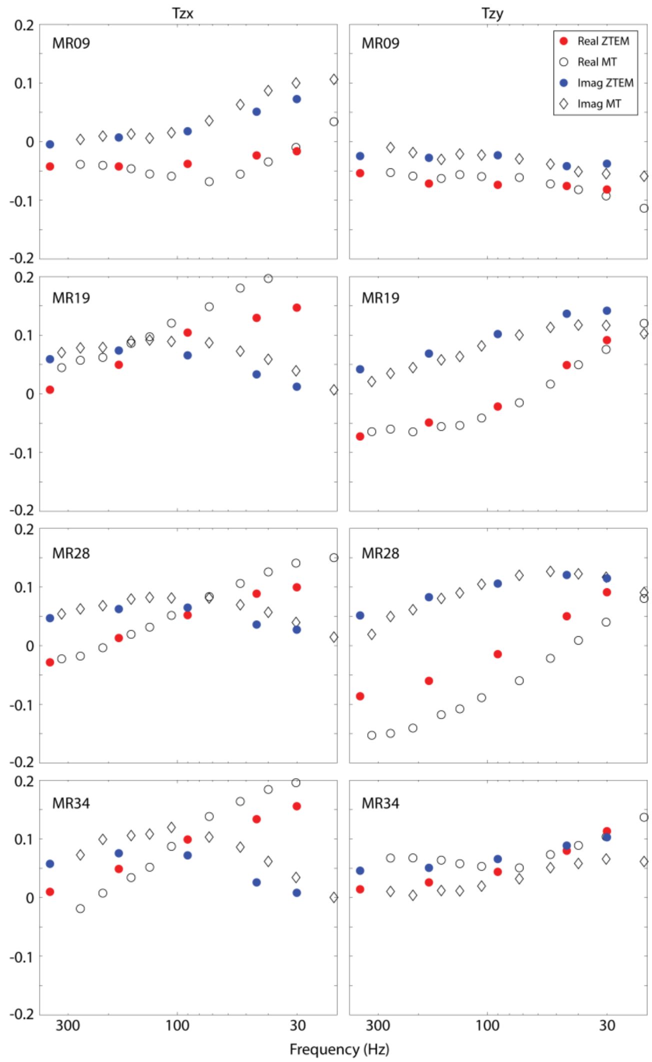

Figure 5: Comparison of airborne ZTEM (solid colored circles) and ground MT (open circles and diamonds) at four MT stations. The left column shows the T_{zx} component and the right column shows T_{zy}. Although the response magnitudes are not exactly the same, the ZTEM and MT data show the same trends at overlapping frequencies. MT data error bars are smaller than the plotted data points and are not shown.

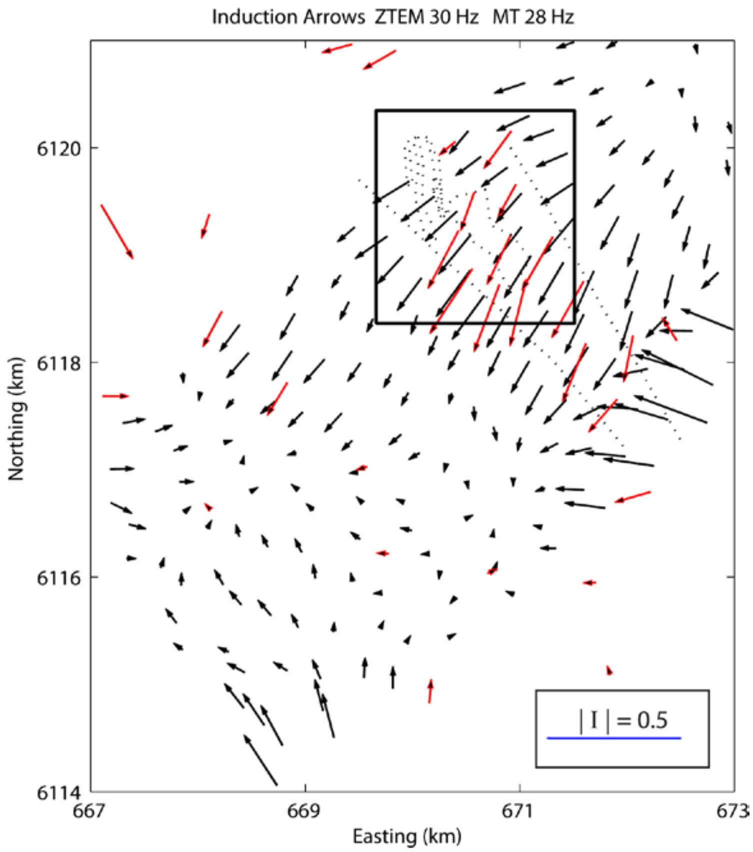

Figure 6: Comparison of induction arrows from the ZTEM survey (black arrows) and the MT survey (red arrows) at comparable frequencies. There is good agreement particularly over the Morrison deposit where induction arrows point toward the southwest. Arrows are shown in the Parkinson convention. Dotted lines are the Morrison orebody, 3 biotite-feldspar porphyry dikes, and the Morrison Graben. The black box is the deposit area shown in Figure 3B.

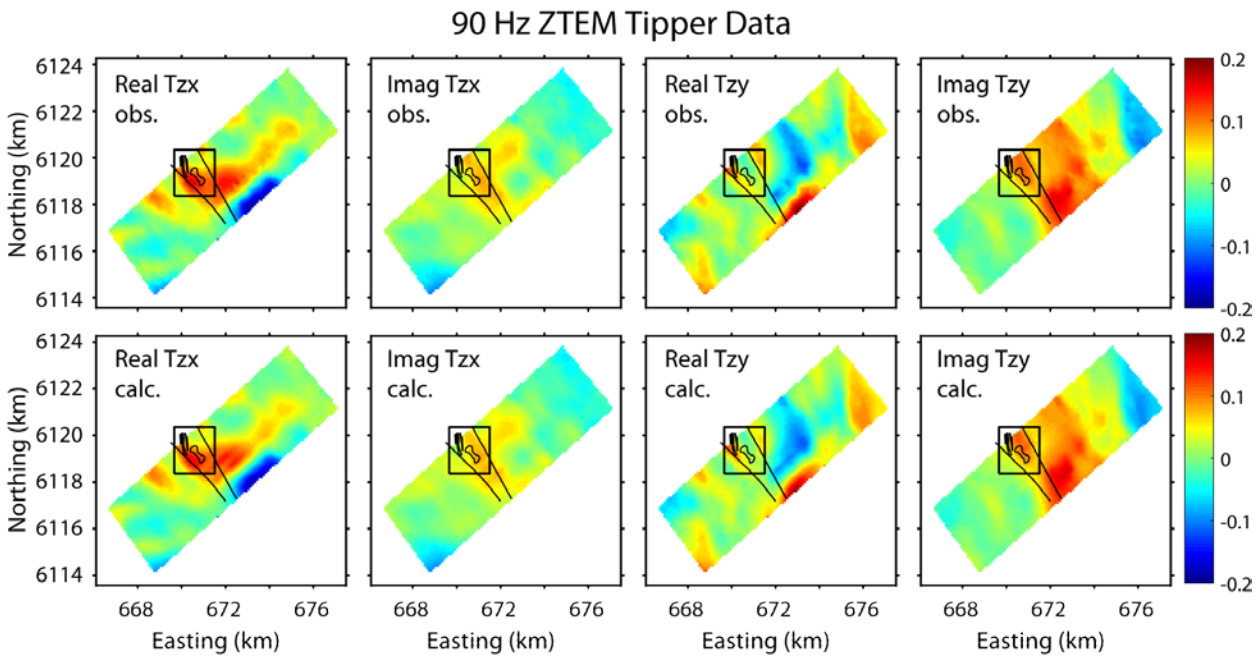

Figure 7: Map view of observed and calculated data at 90 Hz from the ZTEM inversion. The Morrison orebody, 3 biotite-feldspar porphyry dikes, and the Morrison Graben are outlined with black lines. The black box is the deposit area shown in Figure 3B.

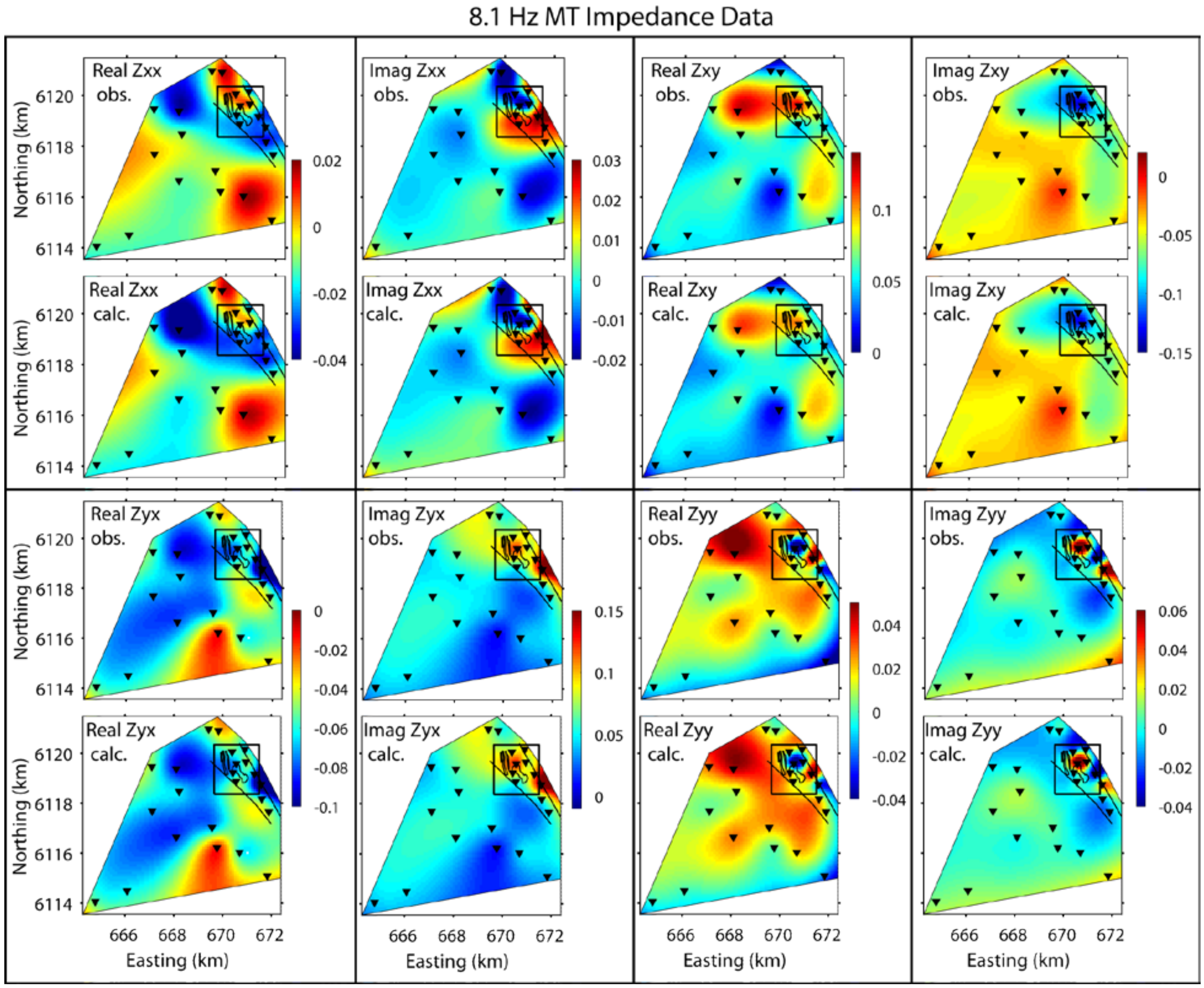

Figure 8: Map view of observed and predicted data at 8.1 Hz for the MT inversion. The real and imaginary parts of the four impedance components (*xx*, *xy*, *yx*, and *yy*) are shown. Black triangles are locations of the MT stations. The Morrison orebody, 3 biotite-feldspar porphyry dikes, and the Morrison Graben are outlined with black lines. The black box is the deposit area shown in Figure 3B.

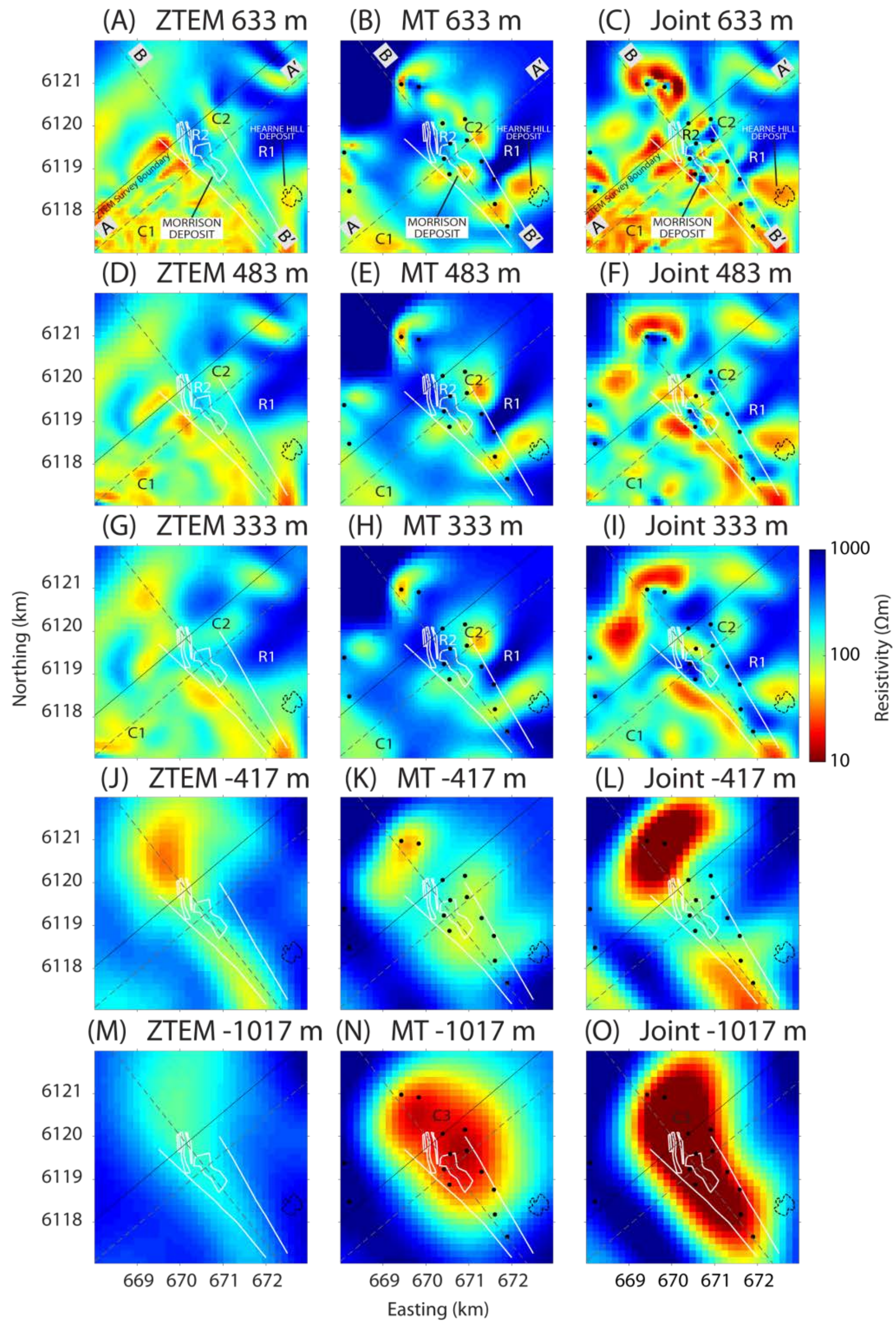

Figure 9: Horizontal slices through ZTEM inversion model (A,D,G,J,M), MT inversion model (B,E,H,K,N), and joint ZTEM-MT inversion model with $\gamma = 3$ (C,F,I,L,O) at 633 m, 483 m, 333 m, -417 m, and -1017 m elevation above sea level. The elevation at the Morrison deposit is about 800 m above sea level. The Morrison orebody and 3 biotite-feldspar porphyry dikes are outlined in white, along with the bounding faults of the Morrison Graben. The Hearne Hille deposit is outlines in black. Black dots are MT station locations. A-A' and B-B' are the profiles for the vertical sections shown in Figure 10. The resistive feature R2 and the conductive C2 may be associated with hydrothermal alteration, and appear in both the ZTEM and MT models. C1 and R1 are consistent with the known deposit lithologies. C3 is a deep conductor that is not imaged in the ZTEM model.

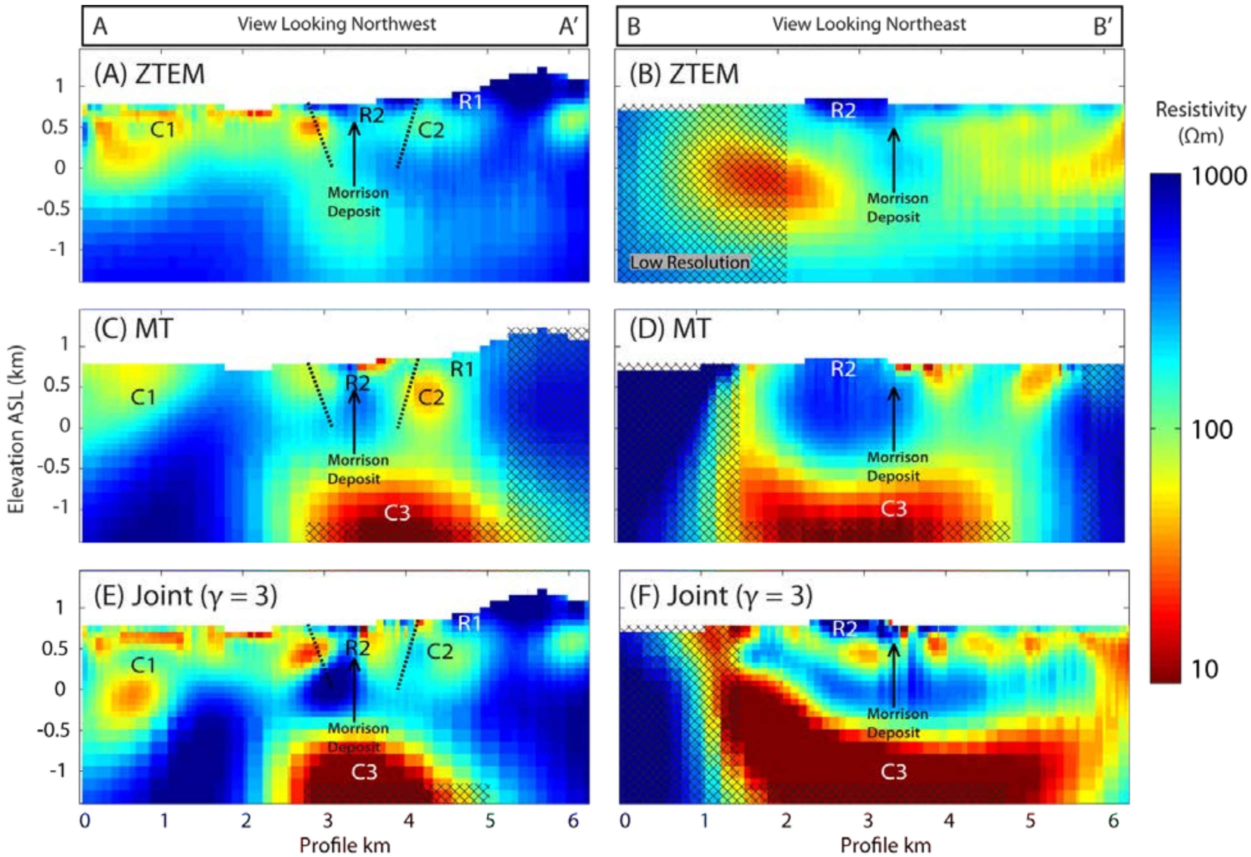

Figure 10: Vertical slices through resistivity models obtained for the ZTEM-only inversion (A,B), MT-only inversion (C,D), and joint ZTEM-MT inversion (E,F) with $\gamma = 3$. Dashed black lines are the approximate location of the Morrison Graben. A,C,E are slices through the profile A-A’ and B,D,F are slices through the profile B-B’ shown in Figure 9. Shaded areas have limited resolution due to insufficient data coverage.

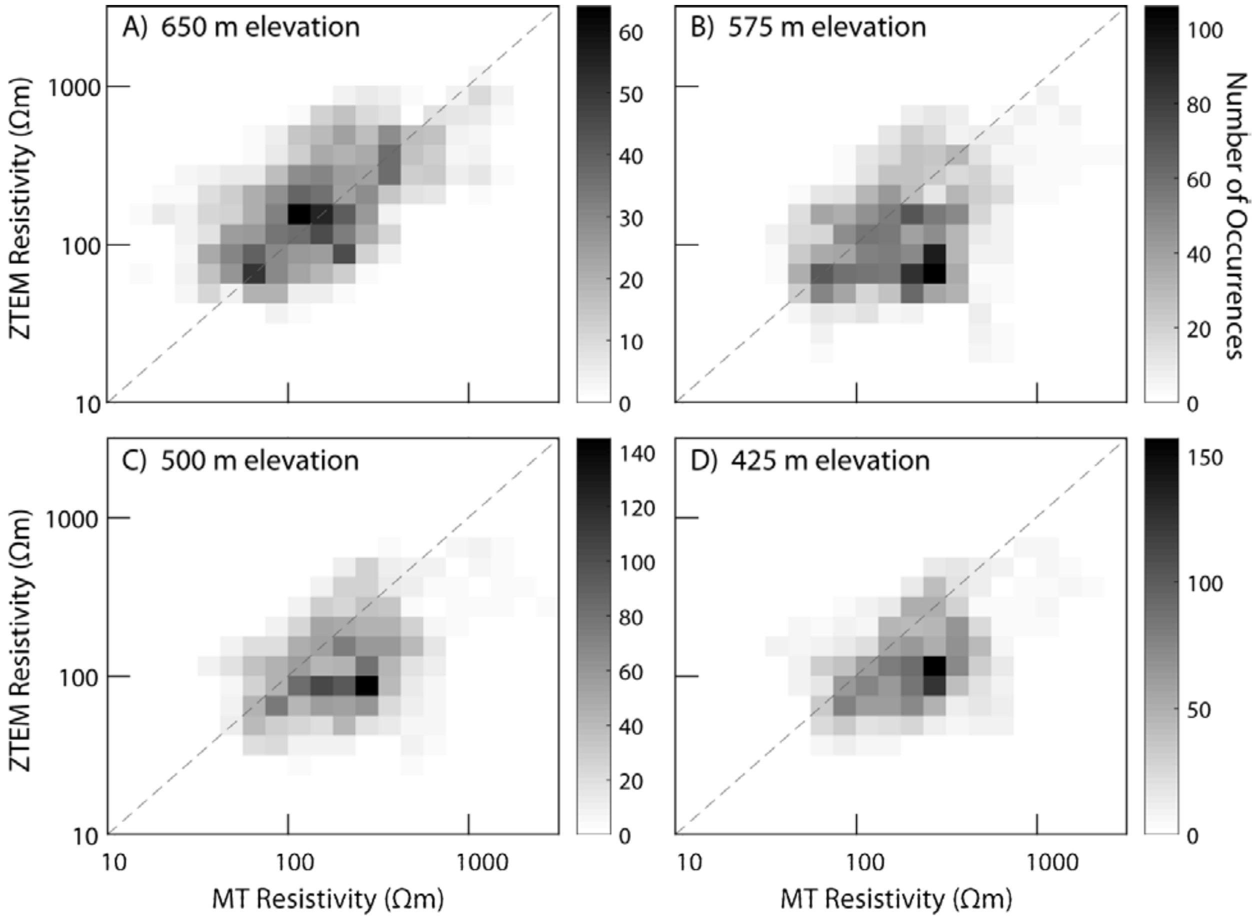

Figure 11: Cross-plots for the preferred ZTEM and MT inversions. Using the same mesh, the resistivity of each cell from the ZTEM and MT inversions was plotted at four depths. Darker squares correspond with more occurrences within a specific bin. The dashed grey line is a one-to-one correlation. At all depths the darker squares (more correlation) occur close to the one-to-one line.

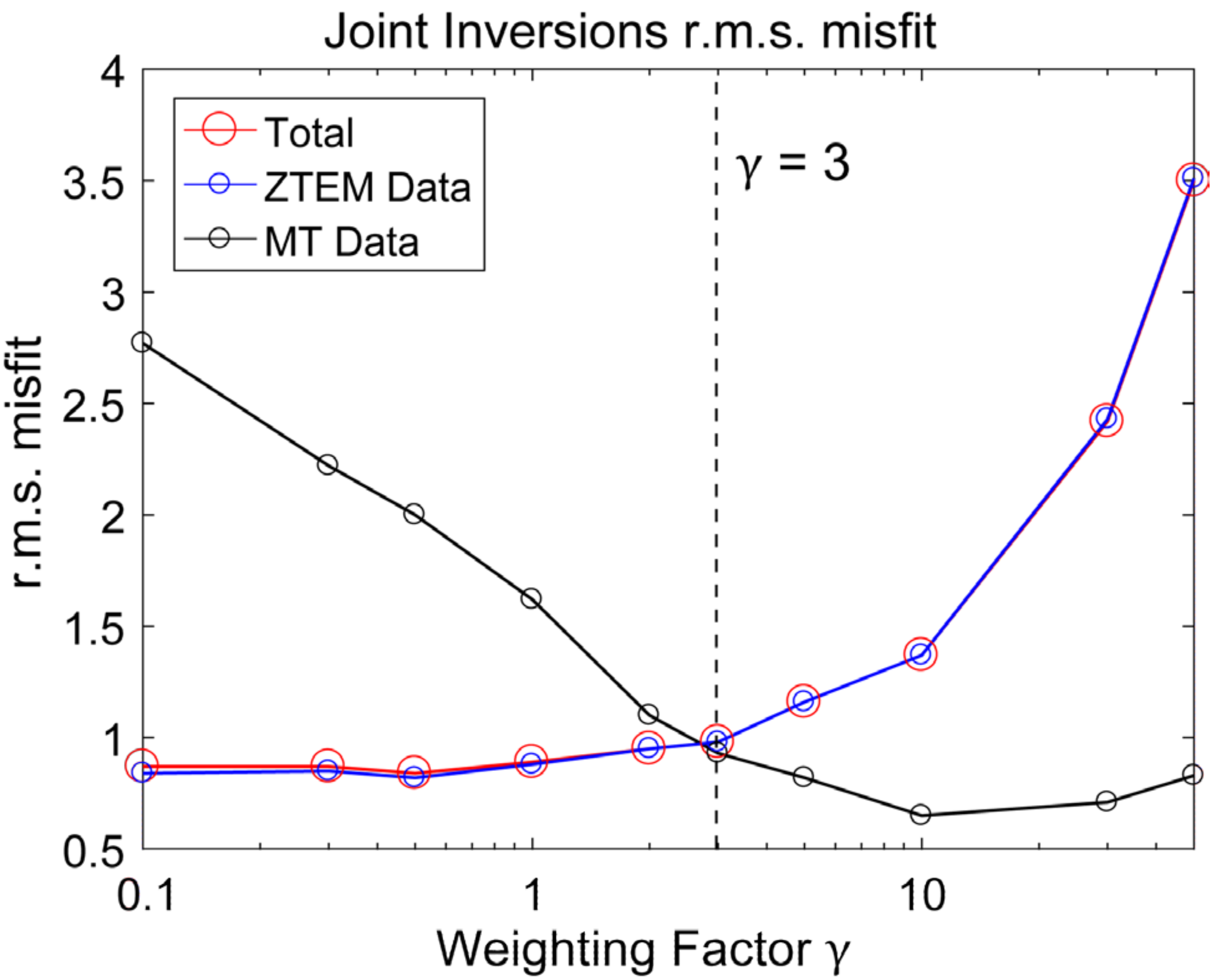

Figure 12: Joint inversion r.m.s. misfit for several trial values of γ. The total r.m.s. misfit as well as the r.m.s. misfit for the ZTEM and MT data subsets are shown for each inversion. The total misfit closely follows the ZTEM misfit because the ZTEM data make up the majority of the joint ZTEM-MT dataset. The dashed line indicates the preferred inversion with $\gamma = 3$.

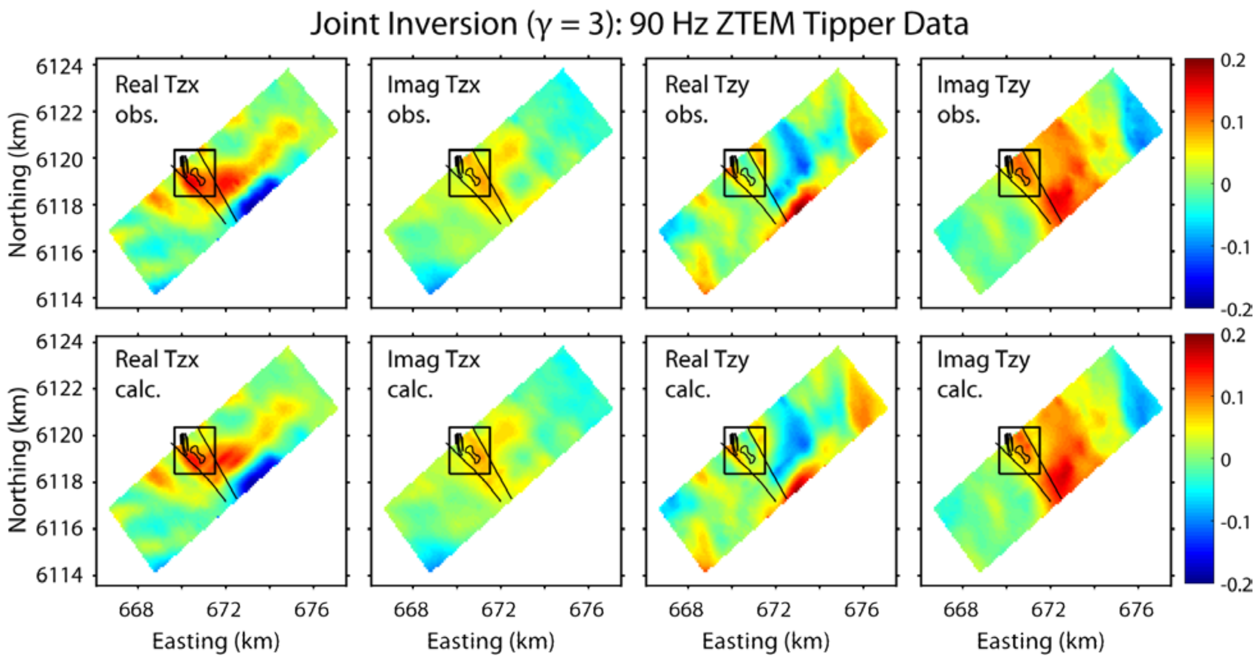

Figure 13: Map view of observed and calculated ZTEM data at a frequency of 90 Hz in the joint inversion with $\gamma = 3$. The Morrison orebody, 3 biotite-feldspar porphyry dikes, and the Morrison Graben are outlined with black lines. The black box is the deposit area shown in Figure 3B.

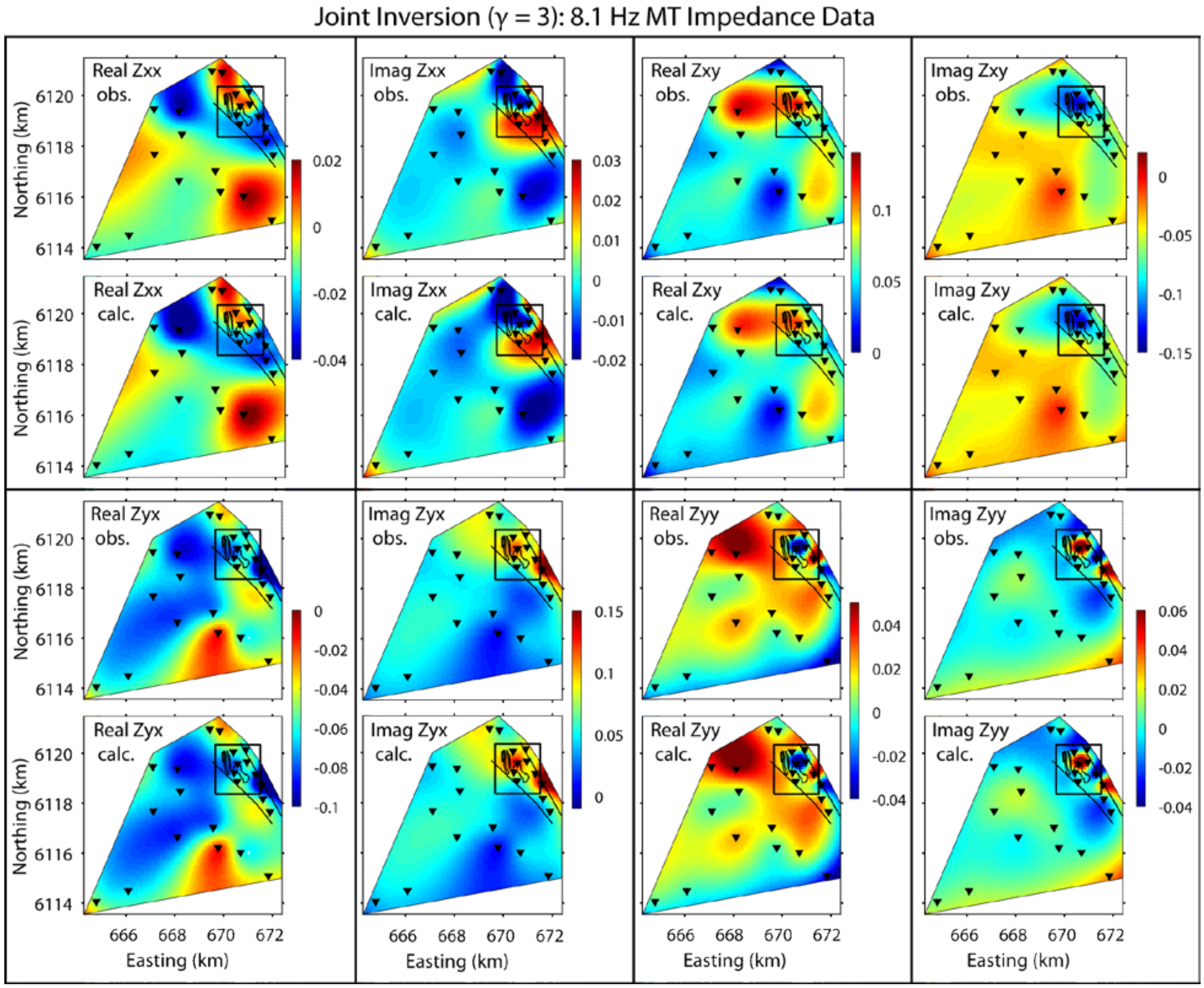

Figure 14: Map view of observed and calculated MT data at a frequency of 8.1 Hz in the joint inversion with $\gamma = 3$. The Morrison orebody, 3 biotite-feldspar porphyry dikes, and the Morrison Graben are outlined with black lines. The black box is the deposit area shown in Figure 3B.

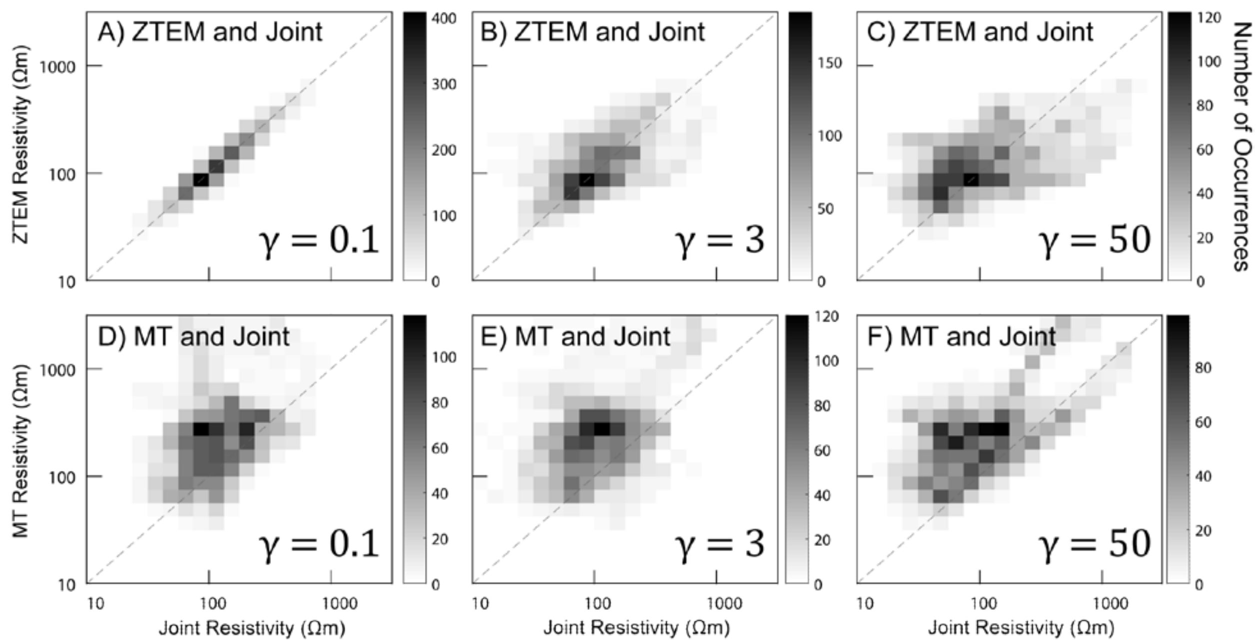

Figure 15: Cross-plots showing correlation in resistivity values at 425 m elevation in resistivity models. A one-to-one correlation is represented by the dashed line in each panel. (A) compares the ZTEM inversion to the joint inversion using γ = 0.1, and (C) compares the ZTEM inversion to the joint inversion using γ = 50. There is a strong correlation between the joint inversion with γ = 0.1 and the ZTEM inversion, but the correlation is weaker with γ = 50. With a low weight on the MT data, the scatter in (D) suggests this joint inversion model does not correlate well with the MT inversion. Stronger correlation is observed in (F) when γ = 50, meaning a higher weight on the MT data. (B) and (E) show that the model using $\gamma = 3$ is a balance between the ZTEM and MT data.

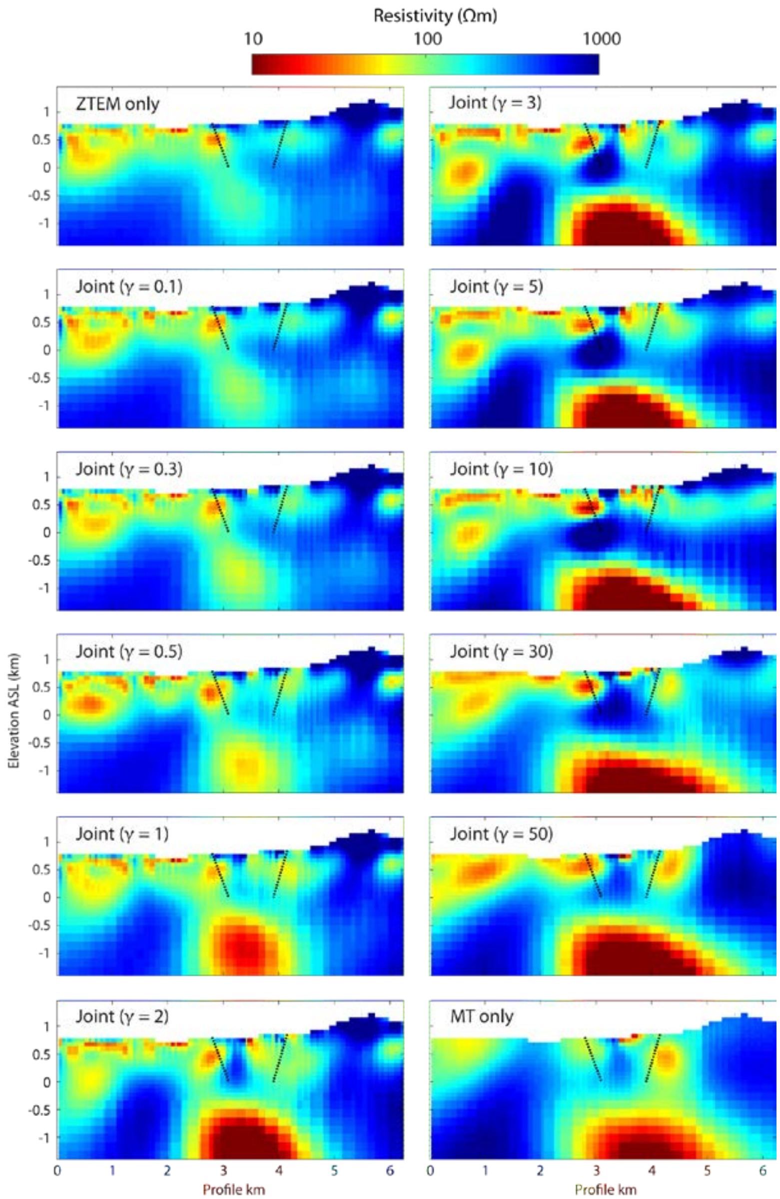

Figure 16: Vertical slice through profile A-A' of joint ZTEM-MT inversions using different γ. The ZTEM and MT models are also shown for reference. With a low γ the joint resistivity model is more similar to the ZTEM model, and with a high γ the model is more similar to the MT model.

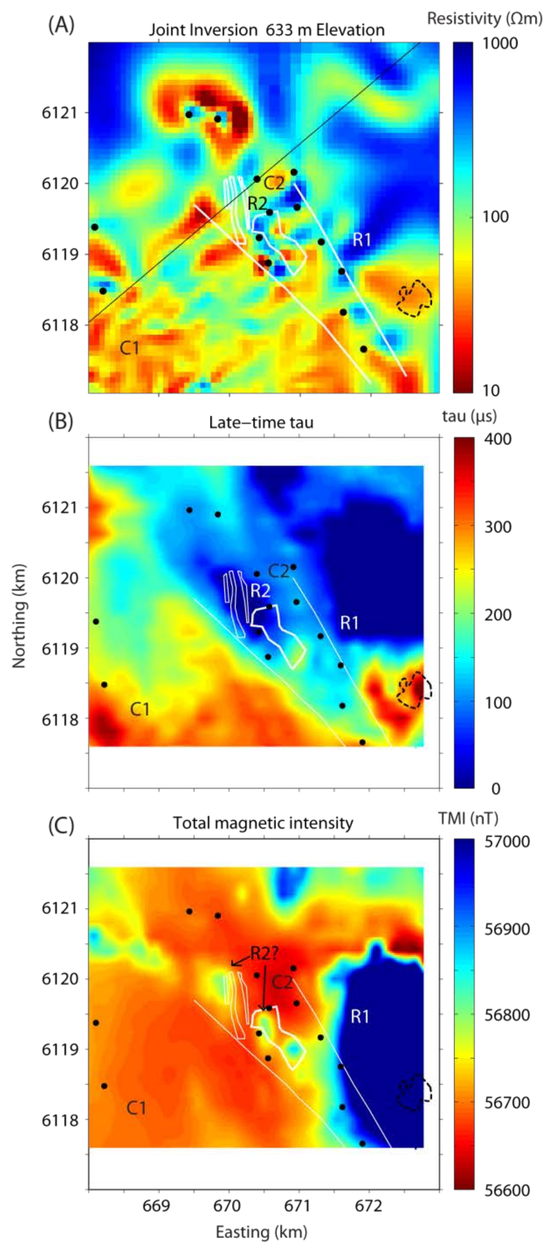

Figure 17: Comparison of A) joint ZTEM-MT inversion resistivity model, B) AeroTEM late-time tau data, and C) airborne total magnetic intensity map of the Morrison deposit. The colorbar is reversed in B) so that red is conductive. The Morrison orebody, biotite-feldspar porphyry dikes, and the Morrison Graben are outlined in white and the Hearne Hill deposit is outlined in black. Tau and magnetic data from Aeroquest Surveys (2009).

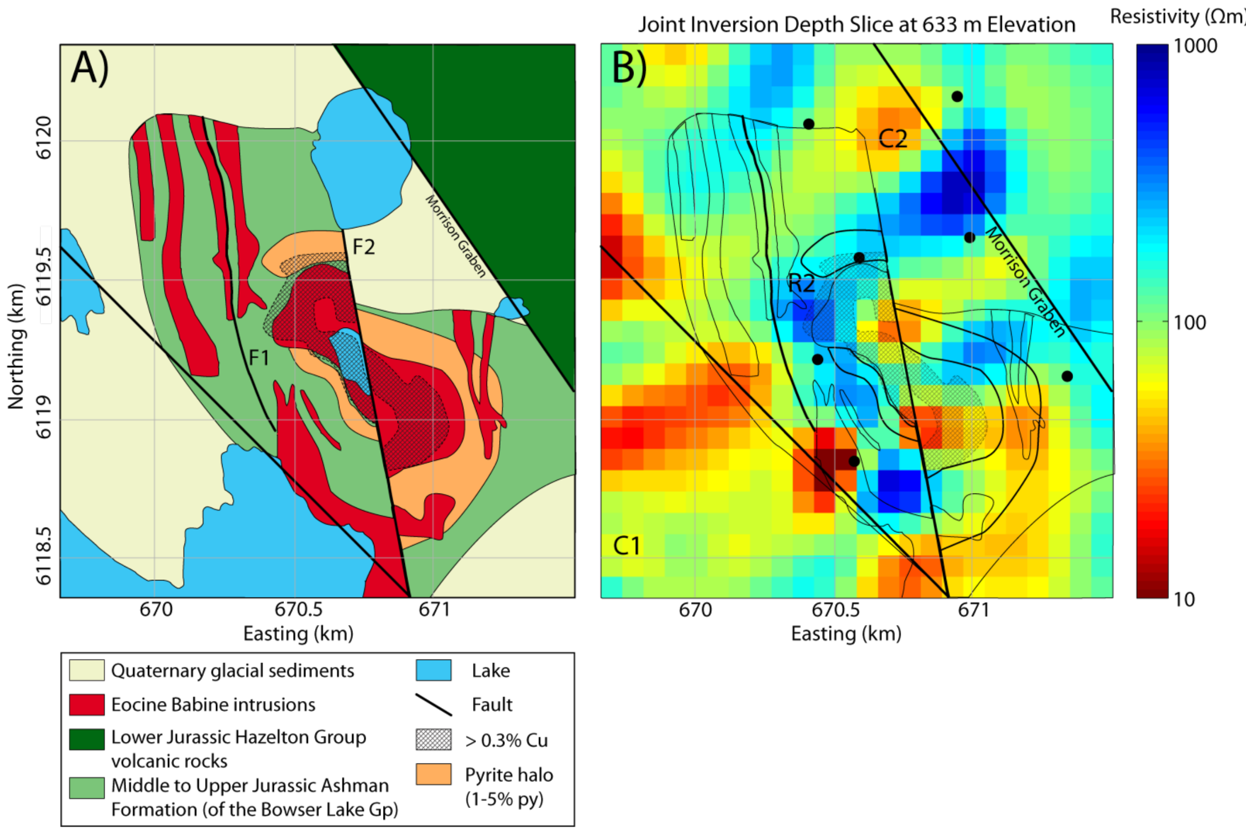

Figure 18: Comparison of Morrison deposit alteration and mineralization map with the joint inversion model. The model slice is about 150 m below the surface. Modified from Liu (2016).

Feature	Geology or Alteration	3-D ZTEM (resistivity)	3-D MT (resistivity)	3-D Joint ZTEM-MT (resistivity)	AeroTEM (tau)	Aeromagnetic (Total magnetic intensity)
R1	Lower Jurassic Hazelton Gp volcanic and sedimentary rocks	High	High	High	Low	High
R2	Potassic alteration assoc. with Eocene Babine intrusive rocks	High	High	High	Low	Moderate
C1	Quaternary glaciolacustrine fill	Low	Low	Low	High	Low
C2	Lake sediments, or faults	Moderate	Low	Moderate	Moderate	Low
C3	Morrison Graben faults or deeper sulfide zone?	Not present	Low	Low	Not present	Not present

Table 1: Resistivity features at the Morrison deposit. The second column indicates the geology or alteration interpreted to cause the resistivity feature. Columns 3 – 7 show whether or not the features were present in various geophysical studies. The length of each bar approximates the value of resistivity, tau, or susceptibility. Colors for the tau data have been reversed so that red is more conductive.

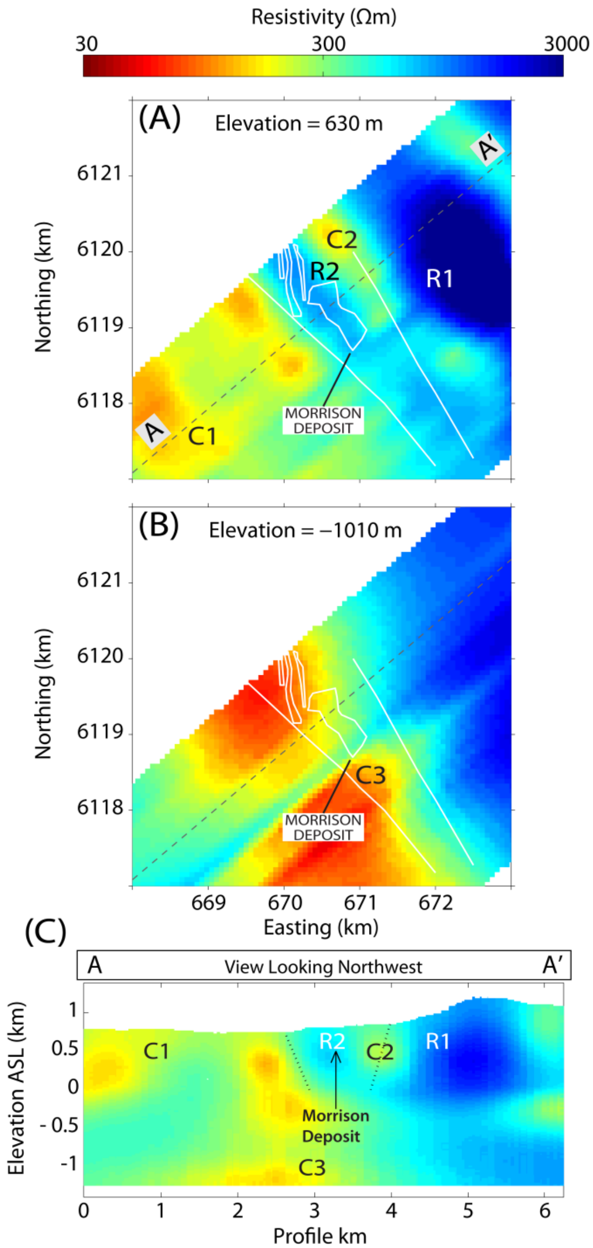

Figure A1: Horizontal slices (A,B) through the resistivity model obtained from 2-D ZTEM inversions (Geotech, 2010). The inversions were performed along flight lines that are approximately 250 m apart. The elevation at the Morrison deposit is about 800 m above sea level. The Morrison deposit and 3 biotite-feldspar porphyry dikes are outlined in white, along with the bounding faults of the Morrison Graben. The vertical slice in (C) is from the 2-D inversion along profile A-A'. C3 is a more prominent feature than in the 3-D ZTEM inversion.

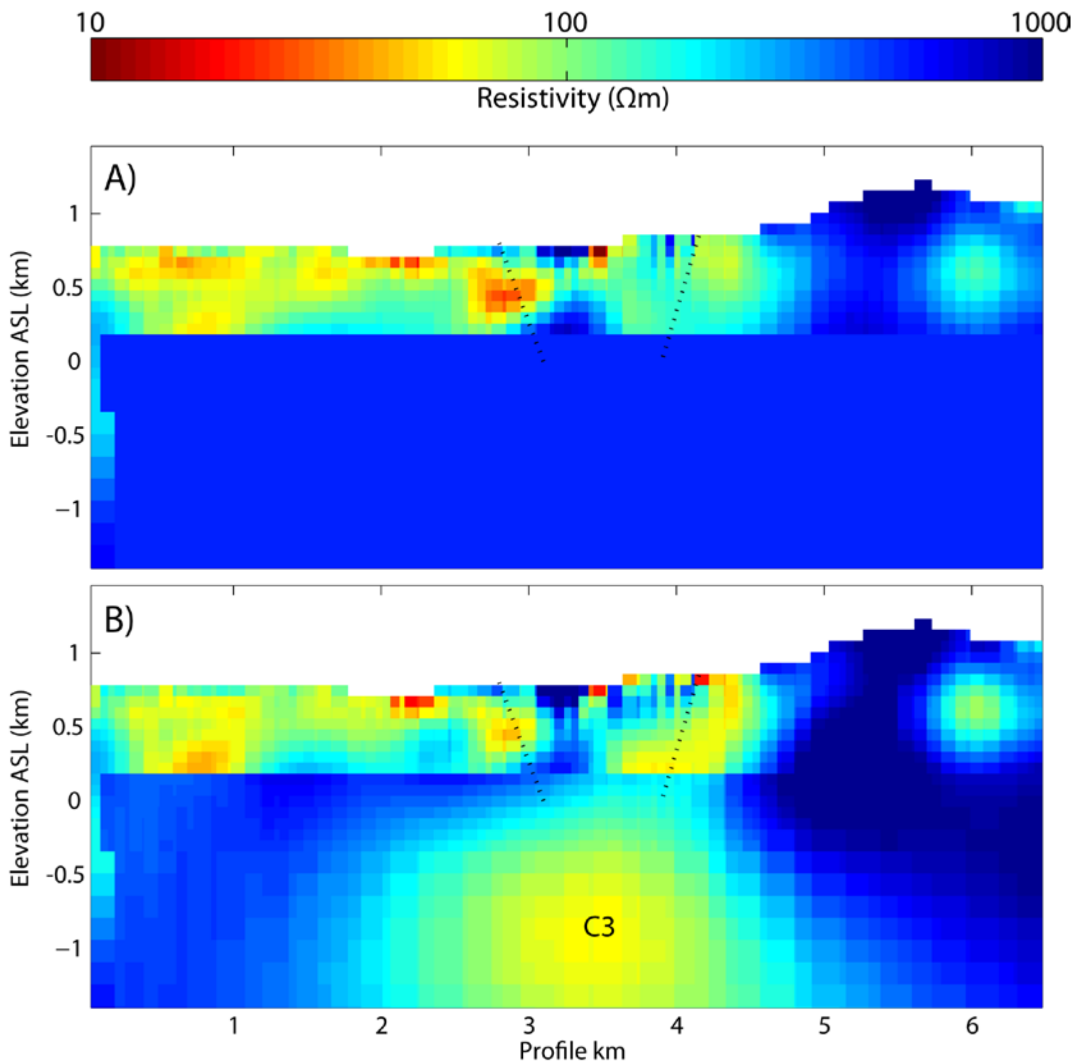

Figure A2: Sensitivity test for the feature C3 seen in the MT and joint resistivity models. In A) an iteration of the joint inversion was selected just before convergence, and C3 was replaced by the background 500 Ωm resistivity. When A) is used as the starting model, C3 is still a required feature after nine iterations as seen in B).